

MULTI-STAGE LINEAR SLOT VIRTUAL IMPACTOR  
FOR CONCENTRATION OF BIOAEROSOLS

A Thesis

by

SHAWN CHARLES CONERLY

Submitted to the Office of Graduate Studies of  
Texas A&M University  
in partial fulfillment of the requirements for the degree of

MASTER OF SCIENCE

May 2005

Major Subject: Mechanical Engineering

MULTI-STAGE LINEAR SLOT VIRTUAL IMPACTOR  
FOR CONCENTRATION OF BIOAEROSOLS

A Thesis

by

SHAWN CHARLES CONERLY

Submitted to Texas A&M University  
in partial fulfillment of the requirements  
for the degree of

MASTER OF SCIENCE

Approved as to style and content by:

---

Andrew R. McFarland  
(Chair of Committee)

---

Dennis L. O'Neal  
(Member)

---

Yassin A. Hassan  
(Member)

---

Dennis L. O'Neal  
(Head of Department)

May 2005

Major Subject: Mechanical Engineering

## ABSTRACT

### Multi-Stage Linear Slot Virtual Impactor for Concentration of Bioaerosols. (May 2005)

Shawn Charles Conerly, B.S., The University of Texas at San Antonio

Chair of Advisory Committee: Dr. Andrew R. McFarland

Two linear slot virtual impactor arrangements were developed and investigated in this study. Both arrangements encompassed two-stage impaction for concentration of bioaerosols. The first arrangement consisted of eight linear slot impactors in parallel for the first stage with the designed dimensions of 87 mm (3.4") for the throat length, 0.305 mm (.012") for the accelerator throat width, and 0.457 mm (.018") for the receiver throat width. The second stage contained a single unit with the designed dimensions of 71 mm (2.8") for the throat length, 0.36 mm (0.014") for the accelerator throat width, and 0.49 mm (0.019") for the receiver throat width. The second arrangement contained a single impactor for the first stage with a designed throat length of 87 mm (3.4"), a designed accelerator throat width of 0.43 mm (.017"), and a designed receiver throat width of 0.63 mm (.025"). The second stage also contained a single impactor with a designed throat length of 8.73 mm (3.4"), a designed accelerator throat width of .43 mm (.017), and a designed receiver throat width of 0.63 mm (0.25").

To verify the tolerances of the machined impactors, optical measurements were made. Both arrangements were subjected to liquid and solid particle tests and have a theoretical concentration factor of 100X. The arrangements were tested at flow rates that ranged from 10 L/min to 1000 L/min, where the collection efficiency of the minor flow was determined. An unknown acoustical phenomenon was present during aerosol tests at elevated flow rates causing low minor flow collection efficiencies. In order to test the impactors at elevated flow rates, the acoustical generation phenomenon was systematically studied and suppressed. The cutpoint for the first arrangement was 1.3

$\mu\text{m AD}$ , and the cutpoint for the second arrangement was  $1.0 \mu\text{m AD}$ . The average  $\text{Stk}_{50}$  for both arrangements was 0.71. The throat velocity through the impactors ranged from 21.8 m/s to 73 m/s, and the peak efficiency for these specific throat velocities ranged from 99% to 74%, respectively.

## ACKNOWLEDGEMENTS

Funding for this study was provided by the U.S. Army Research, Development, and Engineering Command (RDECOM), Edgewood Chemical Biological Center (ECBC), under supervision of Dr. Edward Steubing and Dr. Jerry Bottiger (Texas Engineering Experiment Station, Contract Number 32579-60240). As noted by Dr. Steubing, the research efforts of the TEES program are directed to aerosol sampling, concentrating, and collecting phases of the bioaerosol detection problem. Currently, on the national scale, considerable resources are being devoted to the development of new sensors that can rapidly and unambiguously identify bioaerosol agents. These new sensors will need sampling systems to concentrate the particulate matter of the bioaerosol and reliably deliver that particulate matter to the analyzing sensor; however, nationally the non-sensor aspects of bioagent detection have not received proportionate attention. The TEES program provides the opportunity to develop apparatuses that can be integrated with the new sensors in a timely manner. The program provides the basis for upgrading the performance of aerosol processing apparatus used on existing military bioaerosol detection platforms.

I am deeply thankful for this wonderful opportunity to support the mission of ECBC in the bioaerosol detection area. I am extremely grateful to my advisor, Dr. Andrew McFarland, and to the members of my committee for their leadership and guidance. I am also grateful to my colleagues at the Aerosol Technology Laboratory, especially, Dr. John Haglund, Refugio Isaguirre, Clint Adams, Ben Thien, John Vaughan, and Michael Wiley for their unending dedication.

## TABLE OF CONTENTS

	Page
ABSTRACT .....	iii
ACKNOWLEDGEMENTS .....	v
TABLE OF CONTENTS .....	vi
LIST OF FIGURES.....	vii
LIST OF TABLES .....	ix
INTRODUCTION.....	1
DESIGN AND THEORY .....	3
LITERATURE REVIEW.....	6
EXPERIMENTAL PROCEDURE .....	9
Critical Geometry Measurement.....	9
Aerosol Generation Methods.....	10
Aerosol Sampling Procedure.....	13
Multiple Solid Particle Fluorometry Analysis.....	14
Quality Assurance.....	15
Uncertainty Analysis.....	16
RESULTS AND DISCUSSION .....	19
Sound Generation.....	19
Multi-Nozzle Two-Stage Impaction.....	20
Deposition Analysis of EULSI.....	23
Position Variations for EULSI.....	24
100 L/min Two-Stage Impaction.....	25
SUMMARY AND CONCLUSIONS.....	27
RECOMMENDATIONS FOR FUTURE WORK.....	29
REFERENCES .....	30
APPENDIX.....	34
VITA .....	75

## LIST OF FIGURES

	Page
Figure 1. Schematic of virtual impaction. ....	35
Figure 2. Plot of pressure drop inside LSVI #8 for various flow rates.....	36
Figure 3. Breadboard system for multi-nozzle two-stage impactor. ....	37
Figure 4. CAD drawing of EULSI and second stage impactor. ....	38
Figure 5. Exploded view of two-stage virtual impactor. ....	39
Figure 6. Microscopic view of LSVI #20 critical geometry with the two-component putty method.....	40
Figure 7. Flow transport system for solid particles. ....	41
Figure 8. Fluid transport system for liquid particles.....	42
Figure 9. Luminescence vs. wavelength for Duke Scientific green PSL. ....	43
Figure 10. Luminescence vs. wavelength for Duke Scientific red PSL.....	44
Figure 11. Luminescence vs. wavelength for Duke Scientific blue PSL.....	45
Figure 12. Minor flow collection efficiency vs. Stk for LSVI #8 at 37.5 L/min. ....	47
Figure 13. Outlet view of the EUSLI system. ....	48
Figure 14. Minor flow collection efficiency vs. Stk for CSVI #2 with sound suppression device.....	49
Figure 15. Minor flow collection efficiency vs. Stk for LSVI #9 at the tested flow rates. ....	51
Figure 16. Deposition on the throat end of LSVI #9.....	52
Figure 17. 2 $\mu\text{m}$ solid particle deposition for LSVI #9 at 125 L/min. ....	53
Figure 18. Pressure drop inside the EUSLI system at various flow rates. ....	54
Figure 19. Minor flow collection efficiency vs. Stk for EULSI for tested flow rates.....	55
Figure 20. Microscopic view of LSVI #18 critical geometry. ....	56
Figure 21. Minor flow collection efficiency vs. Stk for LSVI #18 at the tested flow rates. ....	57

	Page
Figure 22. Minor flow collection efficiency vs. Stk for two-stage impaction of EULSI.....	58
Figure 23. Minor flow collection efficiency vs. Stk for multi-nozzle two-stage impaction at 300 L/min. ....	59
Figure 24. Plot of wall losses for each impactor inside EULSI. ....	60
Figure 25. EULSI diagram for labeling the various LSVI arrangements. ....	61
Figure 26. Minor flow collection efficiency of 2 $\mu\text{m}$ particles for various LSVI arrangements. ....	62
Figure 27. CAD view of 100 L/min two-stage impactor. ....	63
Figure 28. Exploded CAD view of 100 L/min two-stage impactor. ....	64
Figure 29. Microscopic view of LSVI #13 critical geometry. ....	66
Figure 30. Microscopic view of LSVI #20 critical geometry. ....	67
Figure 31. View of accelerator for second stage impactor. ....	68
Figure 32. Aerosol transport fixtures for second stage impactor. ....	69
Figure 33. Minor flow collection efficiency vs. Stk for LSVI #13 at 100 L/min. ....	70
Figure 34. Minor flow collection efficiency vs. Stk for LSVI #20 at 10 L/min. ....	71
Figure 35. Deposition of 3.3 $\mu\text{m}$ particles on the throat ends of LSVI #20. ....	72
Figure 36. Minor flow collection efficiency vs. Stk for second arrangement against previous impactor results. ....	73
Figure 37. Peak minor flow collection efficiency vs. throat velocity for all tested flow rates. ....	74



## LIST OF TABLES

	Page
Table 1. Illumination intensity for blue, green, and red PSL with different filters.....	46
Table 2. Critical dimensions for EULSI units.....	50
Table 3. List of various models used in LSVI arrangements. ....	61
Table 4. Critical dimensions for LSVI #13, #18, and #20. ....	65

## INTRODUCTION

Given the nature of evolving global biological threats and the proliferation of weapons of mass destruction, a high volume, reliable, and efficient biological point detection platform must be developed. Bioaerosols are defined as airborne particles, large molecules, or volatile compounds that are living, containing living organisms, or were released from living organisms. To detect airborne bacteria cells and spores, viruses, and toxins at relatively real-time and at relatively low concentrations, the aerosol must be pre-concentrated to enhance a detection system's sensitivity. Currently, several apparatuses such as cyclones and impactors are employed to concentrate super micro-meter sized particulates.

One means of achieving aerosol concentration is through the use of a virtual impactor. Virtual impactors were first developed to eliminate the problems generated from particles impacting on the collection surface of a classical aerosol impactor. This problem does not occur in virtual impaction because the virtual impactor does not contain the impaction plate.

The virtual impactor's role is not to collect the aerosol particles; its function is to separate the inlet flow stream into two streams that contain the coarse and fine aerosol fractions. A secondary result, important for the present study, is that the concentration of particles in the coarse aerosol stream is increased by approximately the ratio of total air flow rate to minor air flow rate, usually about 10:1.

Figure 1 shows how the air is accelerated through a converging nozzle (accelerator blades), and once the particle laden airstream flows past the first set of aerodynamic blades, the particles generally follow one of two paths. Some particles in the airstream will enter the minor flow through the receiver blades and continue their

---

This thesis follows the style and format of *Aerosol Science and Technology*.

linear flow path. These particles contain sufficient momentum to penetrate past the ninety degree turn of the streamlines. Small particles will enter the major flow because they do not contain enough momentum and follow, approximately, the streamlines of the major flow. The major flow path consists of two ninety-degree exhaust passages just beyond the accelerator blades, which carry the majority of the fine particles from the separation zone. An induced vacuum on the major and minor flow streams allows the flow to occur. The flow rate in the minor flow ranges in typical practice over a range of 5% to 20% of the overall total flow rate.

A single linear slot virtual impactor can concentrate air, but a series of impactor nozzles in parallel can be employed to sample a high volume of the ambient air. When the impactors are arranged in parallel, higher amounts of particles above the cutpoint will be concentrated because of higher throughput. Employing a second stage virtual impactor will increase the concentration of particles in the minor flow by approximately ten-fold, and this is a major benefit for multi-stage virtual impactor/concentrators. Successive stages of virtual impaction do not remove the coarse fraction of particles that are above the size range of interest (e.g. pollen), where these nuisance particles are still present in the concentrated stream unless a pre-separator in the aerosol inlet is installed to remove them. The work on multi-nozzle virtual impaction is relatively new, and its performance has not been extensively studied.

## DESIGN AND THEORY

The behavior of the virtual impactor requires consideration of the Stokes number (Stk) and the Reynolds number (Re) since they govern particle and gas phase flow behavior, respectfully, in the virtual impactor.

$$Stk_{L_c} = \frac{\rho_p \cdot D_p^2 \cdot C_c \cdot U_o}{18 \cdot \mu_f \cdot L_c}$$

$$Re_{L_c} = \frac{\rho_f \cdot U_o \cdot L_c}{\mu_f}$$

where:

$D_p$  = particle diameter

$\rho_p$  = particle density

$C_c$  = slip correction factor

$U_o$  = mean velocity at acceleration nozzle exit

$\mu_f$  = fluid kinematic viscosity

$L_c$  = critical dimension;  $L_c$  is the nozzle half-width ( $W/2$ ) for  $Stk$  and the full-width ( $W$ ) for  $Re$ .

The Stk primarily governs the collection efficiency in impactor theory. It is the ratio of the particle stopping distance at a mean throat velocity to the throat width. The stopping distance is defined as the maximum distance a particle can travel with an initial velocity in still air without any external forces. For the rectangular slot virtual impactor the throat width is the accelerator nozzle half-width. For a  $Stk \gg 1$ , particles should follow a straight line as the gas turns and for a  $Stk \ll 1$ , particles should follow the gas streamlines. When the Stk is approximately 1, the highest amount of wall losses occur

since this is near the cutpoint. The cutpoint particle size of a virtual impactor,  $Dp_{50}$ , is defined as the aerodynamic particle diameter at which 50% of the particles entering the virtual impactor follow the minor flow stream. It is also defined by Loo and Cork (1988) as 55% for a 10:1 concentrator, where the ratio of the minor flow's efficiency to the sum of the minor and major flow efficiency equals 55%. Likewise, the majority of particles that enter the major flow are below the  $Dp_{50}$ .

Another parameter that can influence the performance of a virtual impactor is the flow Reynolds Number, which defines the ratio of the inertial forces to the viscous forces. The throat width used in calculating the Re in practice is the accelerator nozzle full-width.

For bioaerosol concentration, the pressure drop from moving air through the virtual impactor requires consideration, and it is a function of the acceleration throat velocity.

$$\Delta P = K \cdot \frac{\rho_f \cdot U_o^2}{2}$$

where:

$K =$  the minor loss coefficient

The minimum power required to move air through the virtual impactor is the theoretical power ( $W_{ideal}$ ), neglecting losses from the flow transport system and the blower/pump, and  $W_{ideal}$  is given by:

$$\dot{W}_{ideal} = Q\Delta P$$

where:

$W_{ideal} =$  the ideal power required

$Q =$  total flow rate through the virtual impactor

The theoretical power increases with the square of the nozzle width when the flow rate and cutpoint are fixed in virtual impaction operations. The impactor should be designed to consume less power, but it also should be able to concentrate fine particles. Therefore, minimizing the nozzle width is a vital aspect of the impactor design, so it can consume the least amount of electrical energy.

Once the cutpoint and volumetric flow rate for the first stage virtual impactor are selected, the second stage impactor design is incorporated with a reduced length to maintain a constant cutpoint. Since the flow rate in the minor flow is fixed, the throat length is scaled to maintain a constant cutpoint for both impactor stages but reduce the flow rate through the second stage to 10% of the first stage impactor's total flow rate. The critical dimension is made as small as practically possible to minimize the required blower power.

## LITERATURE REVIEW

The concept of virtual impactor was first introduced by Hounam and Sherwood (1965) and Conner (1966) to overcome limitations with inertial impactors. Early two-stage virtual impactor devices were developed by Loo and Jaklevic (1974) to meet the need to sample and concentrate aerosols from large volumes of atmospheric air. Virtual impactors were further studied by Marple and Chien (1980) while Novick and Alvarez (1987) designed a two-stage virtual impactor called the cascade virtual impactor. Loo and Cork (1988) studied the performance characteristics of the improved virtual impactor in separating particles by size. Chen and Yeh (1987) discussed techniques to minimize internal losses. A high volume virtual impactor for concentrating large amounts of ambient particles was developed by Marple et al. (1990). This device operated at 1130 L/min with a  $Dp_{50}$  of 2.5  $\mu\text{m}$ . Kim and Lee (2000) designed a multi-nozzle virtual impactor, which recorded 14% wall losses for 2.2  $\mu\text{m}$  particles.

As discussed above, an important factor in virtual impactor performance is the pressure drop across the nozzles. An impactor designed by Sioutas et al. (1994), had a nozzle width of .33 cm, but the pressure drop was 30.0 kPa. The pressure drop in the major flow of the Demokritou et al. (2002) impactor design was 5.72 kPa at 45.5 L/min, and the major flow pressure drop for the Ding et al. (2001) impactor was 4.23 kPa at 100 L/min. Romay et al. (2002) developed a round nozzle two-stage virtual impactor, which induced a pressure drop of 3.5 kPa at a Re number of 9500. This relatively extreme pressure drop would require tremendous amounts of electrical energy to operate the impactor, and thus require significant resources over long periods of time. Haglund (2003) described a LSVI with minimum pressure drop, shown in Figure 2. This single nozzle LSVI design was selected as the base element for the multi-nozzle LSVI in this present study. The work of Haglund (2003) on the single LSVI unit demonstrated collection efficiencies greater than 72% for all particle sizes larger than three times the cutpoint (up to a 10  $\mu\text{m}$  aerodynamic diameter) unless the flow rate was higher than 37.5

L/min, at which point an acoustic instability occurred, greatly increasing wall losses and precluding use of the LSVI as a bioaerosol concentrator at flow rates above 37.5 L/min. The term, aerodynamic diameter (AD), is defined for a specific particle as the diameter of a spherical particle that has the density of a water droplet and equal settling velocity as the particle.

The work on multi-nozzle virtual impaction is relatively new, and its performance has not been extensively studied. Kim et al. (2001) studied multi-nozzle two-stage impaction at a flow rate of 1000 L/min with a Re of 24,600 for the first stage and 10,600 for the second stage. Sioutas et al. (1995) developed a three stage fine particle concentrator to increase ambient fine particle concentrations by up to a factor of 30.

The objective of this study was to develop a multi-nozzle virtual impactor (EULSI) with two stages and a cutpoint of approximately 1.3  $\mu\text{m}$ . The design of the two-stage impactor housing system was to be air-tight, as light as practical, and allow the individual linear slot virtual impactor (LSVI) nozzle elements to perform at or near their performance as isolated units. The system was to include a breadboard control system for the multistage concentrator suitable for operation by technical personnel. Figure 3 shows the breadboard system that was operated during multi-nozzle two-stage impaction. The performance (collection efficiency and pressure drop) were studied and compared to previous work. For the multi-nozzle impactor, the study's first stage was to contain multiple linear slot impactor units operated in parallel where the flow rate of each unit was to span from 37.5 to 1000 L/min. The total flow rate to minor flow rate ratio was to be 10:1; however, previous studies have experimented with various ratios. Chang et al. (2001) and Kim et al. (2002) investigated the flexibility of varying minor to total flow ratios for a multi-nozzle impactor. The second stage was to consist of one LSVI unit in series with the first stage units and to be operated at approximately one-tenth of the first stage's total flow rate. Figure 4 shows a CAD view of the multi-nozzle two-stage impactor and Figure 5 shows the exploded view of the same system.



Also a 100 L/min, 1  $\mu\text{m}$  cutpoint two-stage impactor with single units for each stage with a 10:1 total flow to minor flow ratio was also to be developed and studied. In order to study these virtual impactors, the determination of the mechanism and technique for remediation of the acoustic instability observed in the LSVI units in previous studies (Haglund, 2003), was to be analyzed. Characterization of the collection efficiency of each of the system's stages was to be determined independently, and as a combined two-stage device using the breadboard control system for both designs. The results were to be in the form of minor flow collection efficiency for all particle sizes.

## EXPERIMENTAL PROCEDURE

### *Critical Geometry Measurement*

Measurements of nozzle widths and alignment for all studied LSVI units were made to ensure the critical parameters for the impactors were within assumed values of the allowable tolerances. The virtual impactor throat width is the most critical parameter, and it was measured by two different methods. One method for measuring the critical parameters consisted of a 40X magnification microscopic lens with attached camera and distance measuring software. The microscopic lens rendered a clear resolution photograph of the impactor throat width. Photographs of the accelerator and receiver blades were taken from a fixed location. The microscope fine-tuning focus control adjusted the focal point to view either the accelerator or receiver blades. The photographs were next imported into the distance measuring software to calculate the throat width of the accelerator and receiver blades. The offset distance of the two sets of blades was measured, so the value of the impactor misalignment could be determined. As will be seen below, significant offset can cause undesirable particle deposition on the blades.

A second method of critical geometry measurement incorporated a rubber molding material. This two component putty hardens within a few minutes after mixing the two components, allowing a mold of the impactor critical zone to be cast. To prepare the LSVI units for a mold, the units were disassembled and cleaned with isopropyl and water. Then the accelerator and receiver halves were bolted together leaving only the major flow halves disassembled. Rubbing the components in a ball prepared the cast material for making nozzle negatives. After approximately ten seconds the casting material became sufficiently non-elastic to accept an impression of the top of the receiver blades. The accelerator blades were placed on top of the receiver blades and tightly sealed. The mold set for fifteen minutes, after which time, the accelerator was separated from the receiver. The clay did not permanently adhere to the blades and was

easily removed from the blades, leaving an accurate impression of the critical nozzle geometry. A razor blade was used to slice the mold in 2 mm (1/16") thick sections at three locations along the throat length: both ends and the middle. The sections were then viewed and photographed under 40X magnification as described above.

The image produced in this procedure was identical to the geometry of the entire impactor cross section unlike the previous method. Figure 6 shows one such image for LSVI 20. The accelerator width, receiver width, major flow widths, and misalignment values were obtained from one mold. For both methods the impactor throat width and throat length were measured at three locations: first end, opposite end, and the middle. Impactors with values outside assumed tolerance limits were rejected from aerosol testing.

### ***Aerosol Generation Methods***

Two methods of aerosol generation were employed for this study. One method of generating aerosols was accomplished with a Collison nebulizer, (CN311, 6 Jet, BGI, Inc., Waltham, MA). Solid microspheres (Polystyrene Latex, PSL, Duke Scientific, Palo Alto, CA) were used in conjunction with the Collison nebulizer, having sizes ranging from 0.5  $\mu\text{m}$  to 2  $\mu\text{m}$  in diameter. The Collison nebulizer was filled with approximately 60 ml of a distilled water and multi-component PSL suspension. May (1973) specifies that the device can function satisfactorily with an air pressure range of 15-50 psi, but more than  $10^9$  particles/ml of suspension can cause the nebulizer to generate doublets. Once the particle sizes were chosen for this study, the number of particles per ml was obtained for each particle size from the manufacturer. The volume of the microspheres is also known so the amount of each particle size can be determined; keeping the total particles per ml of solution below  $10^9$  particles/ml of solution. A master suspension of at least 2 L was made to ensure multiple tests can be accomplished in a set of replicate experiments. A magnetic stirring bead was inside the sealed master suspension to maintain continuous mixing throughout the experiment. Once a set of experiments began, only the master solution was used to refill the nebulizer for each test as it was

necessary to maintain a constant concentration of test particles. Figure 7 shows the aerosol transport system for solid particles. Once an individual test was completed, the nebulizer was emptied into a separate sealed container, and refilled with approximately 60 ml of the master suspension. This process was repeated until completion of a test set. Since the nebulizer was emptied into a separate container after each test, a new set of tests could then be conducted with the resulting new solution; however, the particle/ml ratio would be different than the original master suspension. Consequently, only one master suspension container was utilized for each particle size because the test aerosol generation rate would vary if the nebulizer solutions were not obtained using the same master suspension.

The other method of aerosol generation was conducted with the use of a Vibrating Orifice Aerosol Generator (VOAG), (Model 3450, TSI Inc., St. Paul, MN). The liquid used in the VOAG was a solution of ethanol, oleic acid, and sodium fluorescein salt (uranine), which is used as an analytical tracer. A master solution of approximately 90% ethanol, 9% oleic acid, and 1% fluorescein by volume was used for particle generation, where the exact concentration was varied to obtain particles of different sizes. To create the master solution, 450 ml of ethanol was measured into two separate containers. Next, 90 ml of oleic acid ( $\rho=0.8935 \text{ g/cm}^3$ ) or 80.415 g was weighed. The oleic acid was added to the first container containing the ethanol and then thoroughly mixed. Next, 10 ml of sodium fluorescein ( $\rho= 1.53 \text{ g/cm}^3$ ) or 15.3 g was weighed and added to the second container of the ethanol and thoroughly mixed. Finally, the two containers were combined and stored in a sealed 1 L container. To remove un-dissolved solids, the solution was filtered through a vacuum filtration device.

With this master solution, the desired particle size was created with the appropriate addition of ethanol. The master solution and VOAG parameters determined particle size:

$$D_p = \left( \frac{6QC_{vol}}{\pi f} \right)^{\frac{1}{3}}$$

$$C_{vol} = \frac{x_{nv}V_{ms}}{V_{ms} + V_{dil}}$$

where:

$D_p$  = particle diameter

$Q$  = liquid volume flow rate

$C_{vol}$  = volume fraction non-volatile material

$f$  = frequency of applied signal

$x_{nv}$  = non-volatile volume fraction of master solution

$V_{ms}$  = volume of master solution

$V_{dil}$  = volume of diluting solution

The VOAG was set up for monodisperse aerosol generation by first flushing the liquid feed system with a full syringe of isopropyl prior to test aerosol generation; the VOAG was then operated according to the manufacturers operating instruction, with respect especially to ensuring an absence of satellite droplet generation by proper adjustment of amplitude and frequency of applied voltage. Care was also taken to fully flush the VOAG at the conclusion of operation. At the conclusion of aerosol generation, the fluid feed system was flushed with isopropyl to ensure the orifice and flow path were clean.

Once a single stream was observed, an Aerodynamic Particle Sizer (APS), (33210, TSI, St. Paul, MN) was utilized to verify the size distribution of the test aerosol. Chen et al. (1990) concluded that this APS is precise for the particle range of this study. Use of the APS combined with proper operation procedures applied to the VOAG ensured that the test aerosol was monodisperse within a few percent.

Once the monodisperse aerosol was generated, a charge neutralizer tube was installed at the VOAG outlet to remove any static charge on the test particles. Additionally, a cleanup blower was employed with the aerosol transport assembly to draw in the aerosol when the reference filter or sample was operated. The cleanup blower prevented the test aerosol from contaminating the aerosol delivery system.

### *Aerosol Sampling Procedure*

For collection of generated monodisperse liquid aerosol, a 47 mm filter was installed in the minor flow of the virtual impaction system. The impaction system was connected to the aerosol transport system with a ball valve preventing the aerosol from entering the impactor prior to the start of the test (Figure 8). To start the test, the impactor's blower was turned on and the ball valve was opened to allow the test aerosol to flow into the virtual impactor system. A stop watch was used to monitor the duration of the test. Upon termination of the test, the impactor blower was turned off. The ball valve was immediately closed to prevent unwanted aerosol from entering the impactor. This process was repeated for each test and for the reference samples.

After collection of the test aerosol on a glass fiber filter (Pall Gelman Sciences Model A/E 47 mm, Ann Arbor, MI), the analytical tracer in the collected aerosol was eluted with a solvent, and the solution was analyzed with a fluorometer (FM109515, Barnstead International, Dubuque, IA) to determine the relative concentration of the tracer. The efficiency was calculated from the ratio of the relative concentration of the impactor sample to the reference sample. The efficiency curve was determined by combining results from the various particle sizes from tests with the Collison nebulizer and the VOAG. The flow rates for the present study ranged from 10 L/min to 1000 L/min with a fixed value of 10% minor flow to total flow ratio for all impactor stages. The test particle diameter range spanned from 0.5  $\mu\text{m}$  to 10  $\mu\text{m}$ , the range of interest for the present study.

Between the reference and sample test, the test aerosol was impacted onto a glass slide for 2 seconds. The glass slide was viewed under a 40X magnification lens to determine the particle size in pixels. The conversion of particle size from pixel units to metric units was 0.169, and this value was calculated from multiple calibration calculations with the stage micrometer. A flattening coefficient of 1.34 for an F coated slide was used by Figueroa et al. (1982) to determine the aerodynamic diameter of the impacted aerosol, and that value was used in this study for the F coated slides.

### ***Multiple Solid Particle Fluorometry Analysis***

Because the manufacturer of the PSL spheres provides particles with three distinct fluorescent tracer colors, it was possible to conduct a single aerosol test with three different sizes of PSL concurrently. Green, red, and blue PSL particles were tested in this study; however, it was necessary to demonstrate orthogonality between the tracers as discussed below.

As noted by the manufacturer, the filters in the fluorometer are used to perform two functions: to allow only light of a specific wavelength to pass into the sample cell and excite a specific molecule, and allow only specific wavelengths to reach a photomultiplier tube.

In the present study, a combined suspension of green, red, and blue PSL particles were prepared for use in the Collison nebulizer. Experiments were conducted in the manner described above for single sized particle suspension. Once the test and reference samples were collected and soaked in ethyl acetate, the appropriate filters were installed in the fluorometer to determine the relative concentration of the red, blue, and green tracer. The following excitation and emission filters were installed to determine the relative concentration measured by the fluorometer: NB 460/NB 490 for the green PSL tracer, NB 540/NB 590 for the red PSL tracer, and NB 360/NB 440 for the blue PSL tracer. Once installed, the relative concentration measured by the fluorometer was 98.6% accurate for the green PSL tracer, 97% accurate for the red PSL tracer, and 98% accurate for the blue PSL tracer. Furthermore, only 1% of the red and 0.33% of the blue PSL tracer, relative to equal concentrations of green PSL tracer, were measured with the above combination of filters for green PSL tracers. 1% of the green and 1% of the blue PSL tracer, relative to equal concentrations of red PSL tracer, were measured with the above combination of filters for red PSL tracer, and only 5.6% of the green and 5.8% of the red PSL tracer, were measured when the above filters were installed for the blue PSL tracer. Figure 9, Figure 10, and Figure 11 show the excitation and emission wavelengths

for the green, red, and blue PSL. Table 1 shows the fluorometry results with each PSL color.

In order to demonstrate the accuracy of the multimodal PSL technique, a verification test was conducted. In the verification test, a PSL suspension was made by combining three drops of green, red, and blue PSL separately with 3.0 mL of ethyl acetate in separate sealed containers. Next, 1 mL of each solution was combined to form a common three color solution. Next, 1 drop of each PSL was combined and stored separately with 3.0 mL of ethyl acetate to form single component reference samples having the equivalent concentration of the respective components in the combined sample. By comparison of the single component reference samples with the combined sample, the cross contamination was determined. Multiple combinations of the fluorometer filters were tested, but only one pair of filters for all three colors produced acceptable results (Table 1). Also, it should be noted that the results were unchanged when the verification test was repeated with various particle sizes from .5  $\mu\text{m}$  to 2.1  $\mu\text{m}$ . Once the correct filters were installed, the fluorometer was set up according to manufacture specifications and the appropriate filters were used to measure the relative concentrations of the tracer components without correction.

### ***Quality Assurance***

Prior to each aerosol test, a pressure decay test was conducted on the impactor and the reference filter assembly. Each was sealed with o-rings, gaskets, and vacuum grease to ensure repeatability and minimum leakage. Once sealed, a vacuum gauge was attached and a 10 kPa (40" H<sub>2</sub>O) vacuum was applied and monitored for decay upon removal of the vacuum source. The time to decay was at least 15 seconds for the vacuum to decrease from 40" H<sub>2</sub>O to 30" H<sub>2</sub>O.

To determine the influence of undesirable background fluorescence in the samples, a background sample consisting of a glass fiber filter soaked in the same solution as the tested samples was measured after zeroing the fluorometer. This procedure allowed for background determination of the fluorescence intensity of filters



and solvents. The maximum observed background reading was 5% over all samples implying a signal to noise ratio no lower than 20:1.

During solid particle testing, a master solution of at least 2 L was made. Since the Collison nebulizer was filled with 60 mL of master solution for each test, all samples and references could be collected with the same master suspension. This suspension was continuously stirred with a magnetic stirrer to ensure adequate mixing. The Collison nebulizer was also continuously stirred during testing to provide relatively constant aerosol generation during each test. After tests were conducted with the nebulizer, it was rinsed with ethyl acetate, isopropyl, and water to remove any residual PSL particles that could be present in subsequent tests.

During liquid particle testing, the VOAG was run continuously. An auxiliary blower collected the generated aerosol during non-testing times. A ball valve was closed and opened at the same time during experiments, where the time was monitored using a digital stopwatch.

### ***Uncertainty Analysis***

To determine the single sample uncertainty, this study incorporated the uncertainty approach of Kline and McIntock. This approach rendered the possible value error from using different instruments to test the virtual impactor. This approach did not offer the uncertainty statistics from repeating an experiment; however, it provided the possible error for each experiment, which is an uncertainty.

$$\eta_{measured} = \left\{ \left[ \frac{FI_t}{FI_r} \right] * \left[ \frac{V_t}{V_r} \right] * \left[ \frac{t_t}{t_r} \right] * \left[ \frac{Q_t}{Q_r} \right] \right\}$$

$$\Delta\eta = \eta \left\{ \left[ \frac{\Delta FI}{FI_t} \right]^2 + \left[ \frac{\Delta V}{V_t} \right]^2 + \left[ \frac{\Delta t}{t_t} \right]^2 + \left[ \frac{\Delta Q}{Q_t} \right]^2 + \left[ \frac{\Delta FI}{FI_r} \right]^2 + \left[ \frac{\Delta V}{V_r} \right]^2 + \left[ \frac{\Delta t}{t_r} \right]^2 + \left[ \frac{\Delta Q}{Q_r} \right]^2 \right\}^{\frac{1}{2}}$$

$$\frac{\Delta\eta}{\eta} = \left\{ \left[ \frac{\Delta FI}{FI_t} \right]^2 + \left[ \frac{\Delta V}{V_t} \right]^2 + \left[ \frac{\Delta t}{t_t} \right]^2 + \left[ \frac{\Delta Q}{Q_t} \right]^2 + \left[ \frac{\Delta FI}{FI_r} \right]^2 + \left[ \frac{\Delta V}{V_r} \right]^2 + \left[ \frac{\Delta t}{t_r} \right]^2 + \left[ \frac{\Delta Q}{Q_r} \right]^2 \right\}^{\frac{1}{2}}$$

$$\frac{\Delta\eta}{\eta} = \left\{ [0.03]^2 + [0.001]^2 + [0.005]^2 + [0.04]^2 + [0.03]^2 + [0.001]^2 + [0.005]^2 + [0.04]^2 \right\}^{\frac{1}{2}}$$

where:

$FI_t$  = fluorometer intensity value for sample test

$FI_r$  = fluorometer intensity value for reference test

$V_t$  = eluted solution volume for sample test

$V_r$  = eluted solution volume for reference test

$t_t$  = total sample test time

$t_r$  = total reference test time

$Q_t$  = observed sample test volumetric flow rate

$Q_r$  = observed reference test volumetric flow rate

The relative uncertainty in the calculation of the collection efficiency was 7%. The variables for this approach were quantities that were directly observed in the course of running each test. The flow rate, pressure drop, and fluorescence intensity values were all observed, but the velocity, Re, Stk, and collection efficiency were calculated from the variables. These quantities were called the results. This approach offered the error to determine the results. The uncertainties for the various instruments utilized in this study were acquired from manufactured reported data, repeated observations, and assumptions for unknown data. The uncertainty for the flowmeters was obtained from the manufacturer (Dwyer Instruments, Inc., Models RMC and RMB, Michigan City, IN) as  $\pm 4\%$  and  $3\%$ , respectfully. The experiments were always repeated and monitored by a digital stop watch, but the user allowed for uncertainties. The timer uncertainties were assumed to be  $\pm 3$  seconds (0.5%). The uncertainty in the throat width was assumed to be  $\pm 0.127$  mm (0.0005) from visual observations under the 40X microscope optical lens. The dimensionless uncertainty of  $\pm 0.01$  was assumed for the flattening factor

when liquid particles were impacted onto a glass slide and analyzed for particle sizing. The observed fluorometer intensity readings varied for each experiment, and the uncertainty attributed to this variation was assumed to be  $\pm 3\%$ . The generation of aerosols from the Collison nebulizer and the VOAG also included uncertainties. The unsteady rate of aerosol generation contributed to the fluorometer intensity variations. Another variable for uncertainty for the fluorometer intensity readings was the repipets. The uncertainty for the liquid dispensers was  $\pm 0.1\%$  which was obtained from the manufacturer.

## RESULTS AND DISCUSSION

### *Sound Generation*

The LSVI unit of Haglund (2003) generated a high pitched sound at flow rates  $\geq 37.5$  L/min. The efficiency of the impactor when sound was present in the system showed low collection efficiency independent of particle size. The LSVI efficiently concentrated particles at flow rates below the threshold of sound generation, but not at flow rates when sound was present. Figure 12 shows the collection efficiencies of LSVI #8 for a flow rate of 37.5 L/min. With this constraint, the maximum operational flow rate for the EULSI was 300 L/min.

This sound generation experienced in this study was a consequence of the configuration of the rectangular slot receiver and the minor flow plumbing. Coltman (1976) studied acoustic disturbances generated by a rectangular jet. Tube walls influence the behavior of the vibrations of the air column because of the viscous and thermal losses across the boundary layer. The physical phenomenon causing wall vibrations in the LSVI was the acoustic pressure in the standing wave of the air column coupled to a vibration mode of the impactor walls. The sound occurs only if there is a reasonably close agreement between the resonance frequency of the wall mode and one of the harmonics of the air-column vibration and if the symmetry of the wall mode is such that the coupling coefficient does not vanish. It is quite easy to satisfy these conditions for an impactor of rectangular cross sections because the local breathing mode in which the impactor cross section tends from a square to a circle can have an arbitrarily low frequency if the walls are thin. The case of pipe of circular cross section is entirely different because the breathing mode involves an actual increase in the local radius of the tube, rather than a simple shape deformation, and therefore has a very high resonance frequency.

A ¼-inch thick rectangular shaped open-cell foam was placed between the LSVI's receiver blades and the minor flow filter holder to prevent sound generation.

This technique was also incorporated on the EULSI. Figure 13 shows the receiver side of the EULSI case. The foam was placed between the adjoining receiver ports. The addition of the acoustic absorbing material eliminated the standing wave and allowed the LSVI's minor flow to transport particles without generating sound. The sound waves traverse back and forth without making contact with a planar surface, so the impactor's design can be tested at elevated flow rates with the premise that it will efficiently concentrate aerosol particles. The sound suppression technique was incorporated into the Aerosol Technology Laboratory's virtual impactors with satisfactory results. Figure 14 shows the satisfactory minor flow collection efficiencies for a circumferential slot virtual impactor for flow rates up to 300 L/min where, without the suppression technique, the successful efficiencies were limited to 130 L/min.

### ***Multi-Nozzle Two-Stage Impaction***

The first process in testing the multi-nozzle two-stage impaction system was to analyze the critical geometry of the individual units that comprise the eight unit first stage impaction system. The process used to measure the units was the optical method discussed above to measure the throat width and misalignment for LSVI units #9 - #17. The average accelerator width was 0.33 mm (0.01318") and the average receiver width was 0.49 (0.01952") for LSVI #9 - #17. The offset width between the accelerator and receiver blades was 0.005 mm (0.0002"). The critical dimensions for all eight units are shown in Table 2.

Once the critical dimensions of the eight LSVI units were determined, aerosol testing was conducted for LSVI #9 to determine the single unit characteristic prior to characterizing all eight units at once. The peak efficiency for LSVI #9 was 99% for a Stk of 16.6. LSVI #9 was tested at a flow rate that spanned from 37.5 to 125 L/min. Figure 15 shows the minor flow collection efficiency vs. Stk for LSVI # 9 at the tested flow rates, and Figure 16 shows the end effects for LSVI #9 at 37.5 L/min. During the tests, deposition was noticed on the ends of the impactor's blades for particles above the cutpoint. Experimental flow visualization studies by Gotah and Masuda (2000) showed

that end effects associated with rectangular geometry virtual impactors decrease the sharpness of the particle collection efficiency curve. Figure 17 shows the 2  $\mu\text{m}$  solid particle deposition for LSVI #9 at 125 L/min. The peak efficiency for LSVI #9 at 125 L/min was 74.4% for a Stk of 5.9. As the throat velocity for LSVI #9 increased, the peak minor flow collection efficiency decreased from 99% to 74.4%. The pressure drop was also measured for the various flow rates mentioned above and is shown in Figure 2. After the single unit LSVI tests were complete, all eight units were placed into the EULSI case and assembled. The above mentioned pressure decay test was conducted prior to each test to ensure repeatability and efficiency.

A pressure drop test was conducted to determine the negative pressure inside the EULSI for the studied flow rates with the results shown in Figure 18. Vacuum in the EULSI case was measured for flow rates over a range of 50 – 1000 L/min. At the designed operating flow rate of 300 L/min, the EULSI pressure drop was 0.5 kPa (2.0"  $\text{H}_2\text{O}$ ), and at 1000 L/min the EULSI pressure drop was 3.24 kPa (13"  $\text{H}_2\text{O}$ ). The EULSI was first tested at a flow rate of 300 L/min and 1000 L/min with 0.5, 1.0, and 2.0  $\mu\text{m}$  PSL particles. Four virtual impactor and three reference samples, for ten minutes each, were collected. The collection efficiency of the EULSI for 2  $\mu\text{m}$  PSL at 300 L/min and 1000 L/min was 61% and 66%, respectively. To draw the necessary flow for the reference samples at 1000 L/min, two 800 W brushless blowers (117418-01, Ametek, Inc., Kent, OH) were connected in series since one blower could not draw the required flow rate due to the flow resistance of the 104 mm glass fiber filter. Next, liquid particles were generated and the EULSI was tested at a flow rate of 300 L/min. Figure 19 shows the minor flow collection efficiency vs. Stk for the EULSI at the tested flow rates with a peak minor flow efficiency of 75% at a Stk of 11.8.

The second stage LSVI (unit #18) critical geometry was analyzed as described above, which revealed the accelerator width to be 0.334 mm (0.01318"), the receiver width to be 0.496 mm (0.01952"), and the misalignment to be 0.013 mm (0.0004"). Figure 20 shows a magnified view of LSVI #18 critical geometry. The pressure decay test and replicated tests, as discussed above, were conducted for the second stage

impactor. Two flow rates were studied for LSVI #18: 36.5 L/min and 100 L/min. These flow rates correspond to 10% of the total flow rate for the previously described test conditions with the EULSI. With a 10% minor flow rate, the aerosol particle concentration increased by 10X. Figure 21 shows the minor flow collection efficiency vs. Stk for LSVI #18 at the tested flow rates. The peak minor flow efficiency at 36.5 L/min was 95%, and the peak minor flow collection efficiency at 100 L/min was 88%. The cutpoint at 100 L/min was 0.65  $\mu\text{m}$ . As mentioned for LSVI #9, aerosol deposition was noticed at the end of the impactor for particles above the cutpoint. The particles below the cutpoint showed no signs of end effects, but these particles impacted the receiver blades. These particles impacted the receiver blades since they did not contain enough momentum to maintain the linear path. The throat velocity inside LSVI #18 at 36.5 L/min and 100 L/min was 23 and 65 m/s, respectively.

The flowmeters generated a restriction for testing the EULSI at a flow rate of 1000 L/min with one blower, so two 800 W brushless blowers were installed. The vacuum profile was recorded for the flow rate range of 100-1000 L/min in 50 L/min increments. After the EULSI vacuum was measured, the blower bypassed the flowmeters and drew air straight from the EULSI. Without the flowmeters, one blower drew the 13" H<sub>2</sub>O from the EULSI case with less electrical energy since a 1 $\frac{1}{4}$ " hose generated less restriction than a  $\frac{1}{2}$ " flowmeter plumbing. This alleviated additional equipment that added to the overall weight of the system. The minor flow was also drawn from the blower by linking a 3/8" tubing to a 1 $\frac{1}{4}$ " tee with a hose that drew air from the major flow of the EULSI. The minor flow was monitored by using a flowmeter, but the restriction of the flowmeter was less than the major flow since the minor flow operated 10% of the total flow rate.

Once both stages were independently tested and studied, two-stage impaction was conducted for the multi-nozzle system. Previous tests of the two-stage impactor showed lower minor flow collection efficiency. The previous tests incorporated a second stage, which did not contain a separate major flow split. It has been observed that when the major flow widths are not commensurate the flow will not be equal within

the two major flows. The pressure remained constant through their respective gaps but not flow rates. For this test a second stage was employed with separated major flows. The flow rate was 300 L/min through the entire system with a 10% minor flow rate. The minor flow for the second stage was also set at 10% of the first stage's minor flow. The first stage minor flow exited through a 1 inch O.D. tube and entered the second stage. After virtual impaction in the second stage, the remaining aerosol in the minor flow was collected on a 104 mm glass fiber filter. The units were cleaned prior to testing, and 3 samples and 3 references were collected. With a 10% minor flow, two-stage impactor, the aerosol was 100X more concentrated in the minor flow than when the aerosol entered into the system. The system was tested at 300 L/min for the first stage and 30 L/min for the second stage. The 10% second stage flow rate rendered a 10X more concentrated aerosol leaving the minor flow of LSVI #18. The overall two-stage impaction system peak efficiency was 53%. Figure 22 shows the minor flow collection efficiency vs. Stk for two-stage impaction, and Figure 23 shows a combined minor flow collection efficiency vs. Stk for the individual and combined system for comparison, where the cutpoint for these virtual impactors was 1.3  $\mu\text{m}$ .

### ***Deposition Analysis of EULSI***

The EULSI was tested at 300 L/min with 5  $\mu\text{m}$  particles to determine the amount of wall losses inside the individual impactors. The LSVI units were placed in the EULSI in increasing numerical order, where LSVI #9 and #17 were the outer units. The test and reference samples were collected for 20 minutes to compare the relative concentrations. After the 20 minute sample of the EULSI was collected, the EULSI was disassembled and all the wall losses on the internal surfaces of the LSVI units were recovered with cotton swabs soaked with isopropyl. Two cotton swabs were used for each LSVI unit and then allowed to dry. The cotton swabs were placed into individual sealed containers and filled with 10 ml of a 50/50 solution of isopropyl/H<sub>2</sub>O and stored for 3 hours while the solution eluted the fluorescent tracer from the cotton swabs. The collected impactor sample and reference sample were also placed in sealed containers and filled with 50 ml



of the 50/50 solution. A correction was made to account for the difference in volume of the swab solutions and filter solutions. The measured relative concentration for the cotton swab solutions was divided by 5 since each container was filled with 10 ml of the 50/50 solution.

Figure 24 shows the wall deposition for each LSVI. The center three units contained more deposition than the outer units. The outside LSVI units contained relatively low amounts of deposition at the ends of the throat near the separation zone. LSVI #9 contained relatively low deposition on the top of the receiver blades after the first turn. LSVI #10 contained relatively no measured deposition. LSVI #11 contained a relatively significant amount of end losses on both ends of the unit. LSVI #12 contained relatively low amounts of end losses but deposition occurred in several locations on top of the accelerator blades and along the throat length. There was also noticeable deposition on the bottom of the accelerator blades and the bottom of the receiver blades along the middle and ends. LSVI #15 contained medium amounts of end deposition, and LSVI #16 and #17 contained relatively low amounts of end deposition.

### ***Position Variations for EULSI***

A combination of LSVI arrangements inside the EULSI were tested to determine affect of the number of LSVI units on wall losses with 0.5, 1.0, and 2.0  $\mu\text{m}$  PSL particles. Figure 25 shows the various labeling system for the eight possible LSVI placements, and Table 3 lists the various LSVI arrangements that were studied. Figure 26 shows the minor flow collection efficiency for the various LSVI arrangements. The single LSVI unit was positioned in the center of the EULSI case. Next, a second LSVI unit was placed in the slot next to the first LSVI unit. Another combination of LSVI units was tested by separating the two LSVI units with an empty slot between the two impactors. The next test consisted of three side-by-side LSVI units centered in the EULSI case. When the EULSI was tested with the previously stated LSVI combinations the empty slots were covered with a 1/4-inch adhesive-backed closed-cell foam to ensure all transported aerosol traveled through the impactors. The flow rate was adjusted for

each test to draw 37.5 L/min through each impactor. Three samples and three references were collected for each LSVI arrangement. Before testing was initiated, the above mentioned pressure decay test was conducted to verify proper sealing of the system.

After the initial LSVI arrangements were tested, two different impactors were placed inside the EULSI case for testing. The impactors were placed in the same location as the previous two impactors. The collection efficiency was higher for the second pair of impactors, where the average accelerator widths were lower, and the average offset was less than the first pair of LSVI units. Four impactors were placed in the EULSI with two in the center of the case and two on the outer slots of the case. This arrangement produced the highest efficiency (70%) for 2.0  $\mu\text{m}$ . The efficiency for all 8 impactors in the EULSI case was 60%, and additional impactors were placed in the EULSI case to ascertain the minor flow efficiency after installing the additional impactors. When the additional impactors were placed in the case, the gap between the impactors decreased. A large space between the impactor could not be established with a rigid EULSI case. The space was limited, and adding more impactors consumed more case volume. Testing of 5-8 impactors in the case showed an average minor flow efficiency of 60% for each combination. The collection efficiency increased with each additional impactor when more than 2 impactors were added, and it increased to 70% with 4 LSVI units, but it remained around 60% with the combination for 5 to 8 LSVI units.

### ***100 L/min Two-Stage Impaction***

The second two-stage virtual impactor arrangement that was investigated was comprised of a single unit first stage and single unit second stage. The slot length for the first stage was 87 mm (3.4") and the slot length for the second stage was 8.7 mm (0.34"). Figure 27 shows a CAD view of a 100 L/min two-stage impactor, and Figure 28 shows the exploded CAD view. The flow rate for this system was 100 L/min through the first stage and 10 L/min through the second stage, where the units were measured with the procedure described above and the measured values for LSVI #13, #18, and #20 are

shown in Table 4. Figure 29 shows a critical geometry photograph for the first stage impactor, LSVI #13, and Figure 30 shows a critical geometry photograph for the second stage impactor, LSVI #20. The second stage impactor provided a tapered inlet, so it could gradually draw the aerosol in from a 1.0" O.D. tube. Figure 31 shows a view of the inlet for LSVI #20. The theoretical aerosol concentration with two-stages was 100X. The second stage mounted to the bottom of the first stage housing assembly, and it contained individual flow controls. Figure 32 shows the aerosol transport fixtures for the second stage impactor.

During aerosol testing of the first stage, the peak efficiency for LSVI #13 was lower than the single units of the EULSI system. Also, the second stage impactor contained more visible deposition at the ends of the impactor's blades. The minor flow collection efficiency for LSVI #13 and #20 is shown in Figure 33 and Figure 34. Figure 35 shows a photograph of the liquid particle end effects for LSVI #20 for 3.3  $\mu\text{m}$ . As the throat length decreased for all impactors, the peak minor flow collection efficiency decreased. A two-stage impactor was also tested for these LSVI units that operated in series, and the minor flow collection efficiency peaked at approximately 20%. Figure 36 shows the minor flow collection efficiency for both single stages and the combined two-stage impaction test. More deposition was visible on the throat ends for this arrangement.

## SUMMARY AND CONCLUSIONS

There was several wall loss mechanisms observed with the LSVI based concentrators that must be mitigated to allow for successful bioaerosol concentration. The current linear slot virtual impactor design consists of four sections. The four sections are assembled and bolted together. Vacuum grease is applied to the individual sections where metal contact takes place to ensure a leak tight seal. Since the parts are machined, some infinitesimally small space will exist even after the sections are assembled. When particles are drawn through the accelerator blades of the impactor, larger particles impact the ends of the linear slot. Since the larger particles have a significantly larger momentum they will have a higher chance of not following the streamlines and impact at the throat end. When the throat length decreased from 87 mm (3.4”) to 8.7 mm (0.34”) the peak minor flow collection efficiency decreased from 99% to 31% for an individual LSVI unit.

The EULSI is currently arranged to not draw the particle laden airstream from separate major flow controls. The adjacent major flows share a common port, and the peak efficiency for the EULSI was 75%. The peak efficiency for an individual LSVI unit was as high as 99%, but when the major flows were not separated the peak efficiency decreased. The lack of individual flow control for each LSVI in the EULSI may explain the reduction in minor flow collection efficiency.

An acoustical phenomenon prevented the LSVI units from operating properly, above 37.5 L/min, but with an acoustic suppression technique, the impactors performed as a classical impactor at higher flow rates.

At elevated throat velocities, the virtual impactor collected less aerosol in the minor flow than at lower throat velocities. Figure 37 shows the peak minor flow collection efficiency vs. throat velocity for all tested flow rates in this study. As the throat velocity increased from 22.0 m/s to 73.0 m/s, the peak minor flow collection efficiency decreased from 99% to 74%. This decreased efficiency was valid for 4 of 5

different LSVI throat velocities. Multi-component PSL testing was developed and used in concurrent tests, which allowed the study of three particle sizes in the particle laden air stream. Test setup time was reduced when multiple particle sizes were tested at the same time.

In conclusion, maintaining high collection efficiencies for both the first and second stage will render more concentrated aerosol for detection platforms. Therefore, separating the major flows with individual flow controls will ensure that the minor flow collection efficiency remains high. When the throat velocity was maintained around 22.0 m/s, the highest minor flow collection efficiencies for this type of LSVI were measured.

## RECOMMENDATIONS FOR FUTURE WORK

Developing a bioaerosol concentration device that will consume much less electrical power than contemporary systems (perhaps 1/10 as much) should enable the use of batteries, rather than portable generators, as the energy source to operate the system in the field. When coupled with a collection stage the concentration device should deliver the bioaerosol particles to the sensor in a more rapid and efficient manner than any existing apparatus. There are many difficult problems that must be solved before the point is reached where we can achieve force protection with a lightweight, reliable, and efficient bioaerosol detection apparatus.

An alternate design for the EULSI system was presented. Throughout the testing process, low collection efficiencies were noticed at all flow rates when the major flows were not individually ported. The minor flow collection efficiencies for the individual LSVI units were above 95% when the throat velocity was approximately 22.0 m/s. Prior to each test, the LSVI units were cleaned to remove any debris or contamination. When the throat velocity in the LSVI units increased above 22.0 m/s and throat length decreased from 87 mm (3.4") to 8.7 mm (.34"), the peak minor flow collection efficiency decreased. These inefficiencies contributed to lower minor flow collection efficiency in two-stage virtual impaction. Further development is needed to solve the separate flow and elevated throat velocity issues for the concentration of bioaerosols with LSVI units.

Also, the advancement of a multi-component PSL solution can be further studied. The manufacturer of the PSL that was used in this study only manufactured three different fluorescent tracer particles. The amount of solid particle sizes that can be tested at the same time is dependent on the manufacture's inventory. If a company made more fluorescent tracer particles, then more solid particle sizes could be tested at the same time. This would reduce the experimental setup time that is required to test an individual particle size.

## REFERENCES

- Chang, M-C., Geller, M. D., Sioutas, C., Fokkens, P. H. B., and Cassee, F. R. (2001). Development and Evaluation of a Compact, Highly Efficient Coarse Particle Concentrator for Toxicological Studies, *Aerosol Science and Technology* 36:492-501.
- Chen, B. T., Cheng, Y. S., and Yeh, H. C. (1990). A Study of Density Effect and Droplet Deformation in the TSI Aerodynamic Particle Sizer. *Aerosol Science and Technology* 12:278-285.
- Chen, B. T., and Yeh, H. C. (1987). An Improved Virtual Impactor, *Aerosol Science and Technology* 18:203-214.
- Coltman, J. W. (1976). Jet Drive Mechanisms in Edge Tones and Organ Pipes. *J. Acoust. Soc. Am.* 60:725-733.
- Conner, W. D. (1966). An Inertial-Type Particle Separator for Collecting Large Samples, *J. Air Pollut. Control Assoc.* 1:35-38.
- Demokritou, P., Gupta, T., Ferguson, S., and Koutrakis, P. (2002). Development and Laboratory Characterization of a Prototype Coarse Particle Concentrator for Inhalation Toxicological Studies. *Aerosol Science and Technology* 33:1111-1123.
- Ding, Y., Ferguson, S. T., Wolfson, J. M., and Koutrakis, P. (2001). Development of a High Volume Slit Nozzle Virtual Impactor to Concentrate Coarse Particles. *Aerosol Science and Technology* 34:274-283.

- Figueroa, E. O., McFarland, A. R., and Ortiz, C. A. (1982). Flattening Coefficients for DOP and Oleic Acid Droplets Deposited on Treated Glass Slides. *Am. Ind. Hyg. Assoc.* 43: 395-399.
- Gotah, K., and Masuda, H. (2000). Improvement of the Classification Performance of a Rectangular Jet Virtual Impactor, *Aerosol Science and Technology* 32:221-232.
- Haglund, J. S. (2003). Two Linear Slot Nozzle Virtual Impactors for Concentration of Bioaerosols. Ph.D. Dissertation, Department of Mechanical Engineering, Texas A&M University, College Station.
- Hounam, R. F., and Sherwood, R. J. (1965). The Cascade Centripeter: A Device for Deterring the Concentration and Size Distribution of Aerosols, *Amer. Ind. Hyg. Assoc. J.* 2:122-131.
- Kim, D. S., Kim, M. C., and Lee, K. W. (2000). Design and Performance Evaluation of Multi-Nozzle Virtual Impactors for Concentrating Particles, *Particle and Particle System Characterization* 17:244-250.
- Kim, D. S, Kim, M. C, and Lee, K. W. (2002). An Experimental Study on Aerosol Concentrators: Different Minor to Total Flow Ratios and Various Numbers of Nozzles, *Powder Technology* 127:95-98.
- Kim, M. C., Kim, D. S., Lee, K. W, Youn, H. J., Choi, K. K, and Ha, Y. C. (2001). Multijet and Multistage Aerosol Concentrator: Design and Performance Analysis, *Journal of Aerosol Medicine* 14:245-254.



- Kim, M. C., and Lee, K. W. (2000). Design Modification of Virtual Impactor for Enhancing Particle Concentration Performance, *Aerosol Science and Technology* 32:233-242.
- Loo, B. W., and Cork, C. P. (1988). Development of High Efficiency Virtual Impactors, *Aerosol Science and Technology* 9:167-176.
- Loo, B. W., and Jaklevic, J. M. (1974). An Evaluation of the ERC Virtual Impactor, Report #LBL-2468. Lawrence Berkeley Laboratory, Berkely, California.
- Marple, V. A., and Chien, C. M. (1980). Virtual Impactors: A Theoretical Study, *Environmental Science Technology* 14:976-985.
- Marple, V. A., Liu, B. Y. H., and Burton, R. M. (1990). High Volume Virtual Impactor for Sampling Fine and Coarse Particles, *J. Air Waste Manage. Assoc.* 40:762-767.
- May, K. R. (1973). The Collison Nebulizer: Description, Performance and Application, *Journal of Aerosol Science* 4:235-243.
- Novick, V. J., and Alvarez, J. L. (1987). Design of a Multistage Virtual Impactor, *Aerosol Science and Technology* 6:187-192.
- Romay, F. J., Roberts, D. L., Marple, V. A., Liu, B. Y. H., and Olson, B. A. (2002). A High Performance Aerosol Concentrator for Biological Agent Detection, *Aerosol Science and Technology* 36:217-226.
- Sioutas, C., Koutrakis, P., and Burton, R. M. (1995). A Technique to Expose Animals to Concentrated Fine Ambient Aerosols. *Environmental Health Perspectives* 103:172-177.

Sioutas, C., Koutrakis, P., and Olson, B. A. (1994). Development and Evaluation of a Low Cutpoint Virtual Impactor, *Aerosol Science and Technology* 21:223-235.

APPENDIX

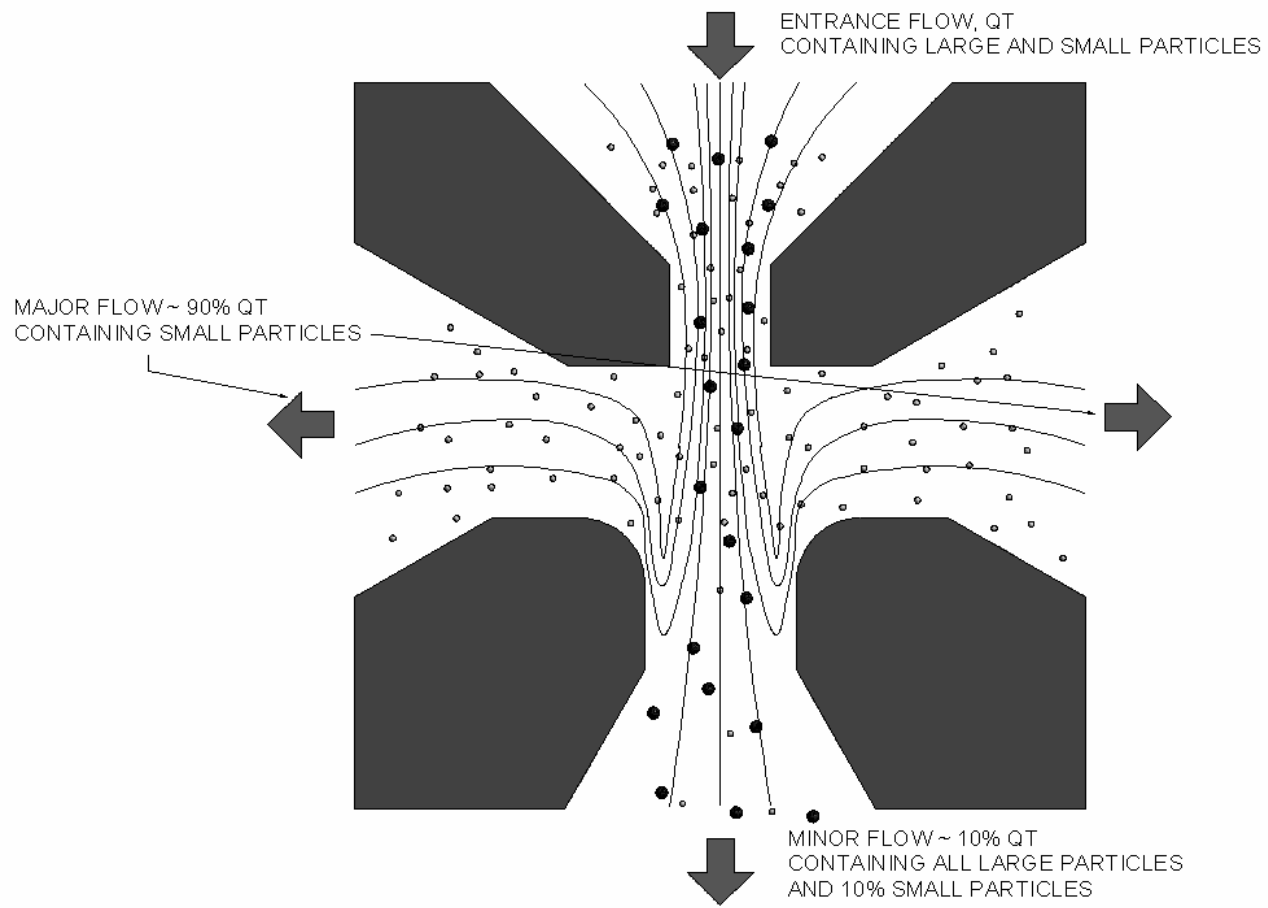


**Figure 1.** Schematic of virtual impaction.

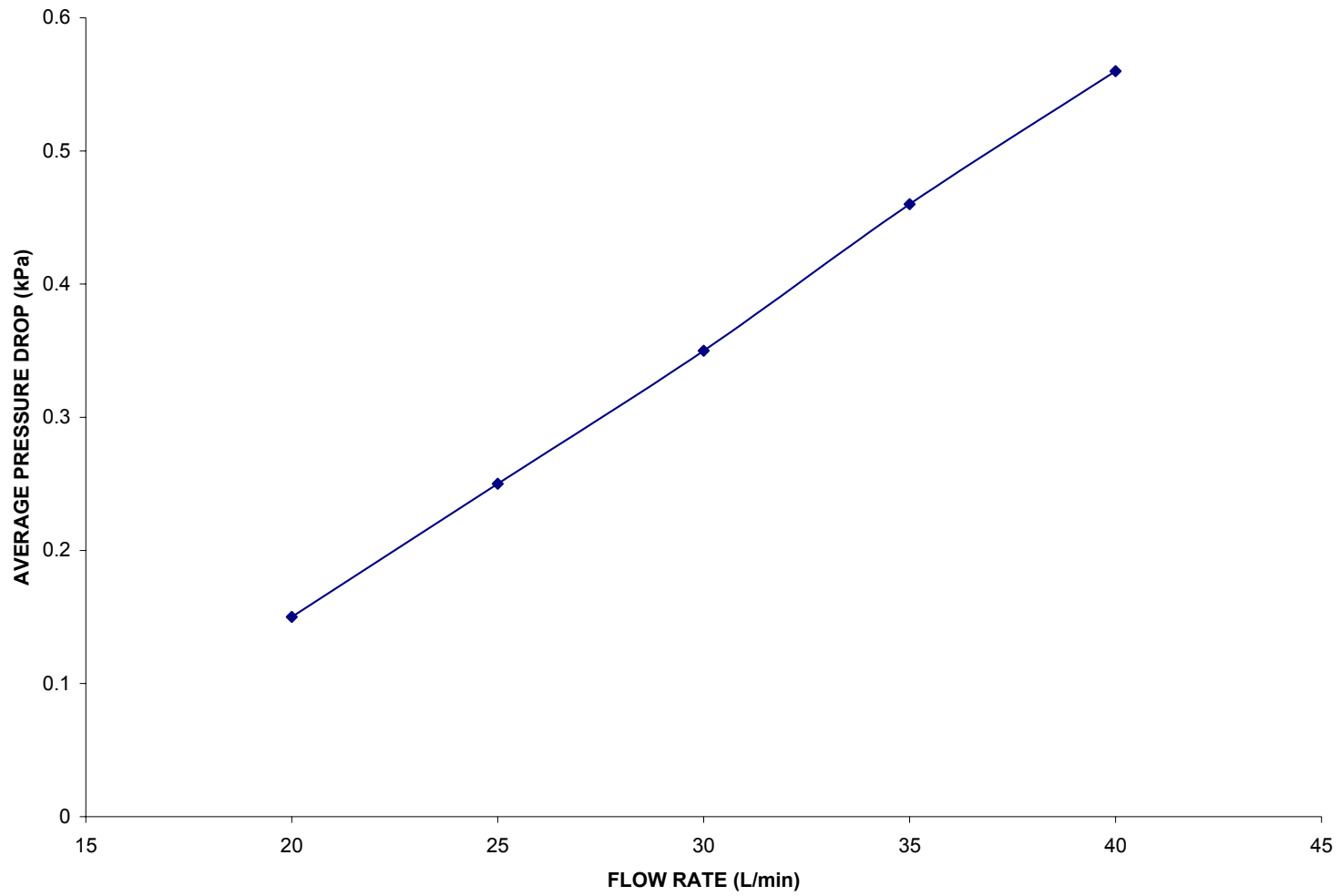


**Figure 2.** Plot of pressure drop inside LSVI #8 for various flow rates.



**Figure 3.** Breadboard system for multi-nozzle two-stage impactor.

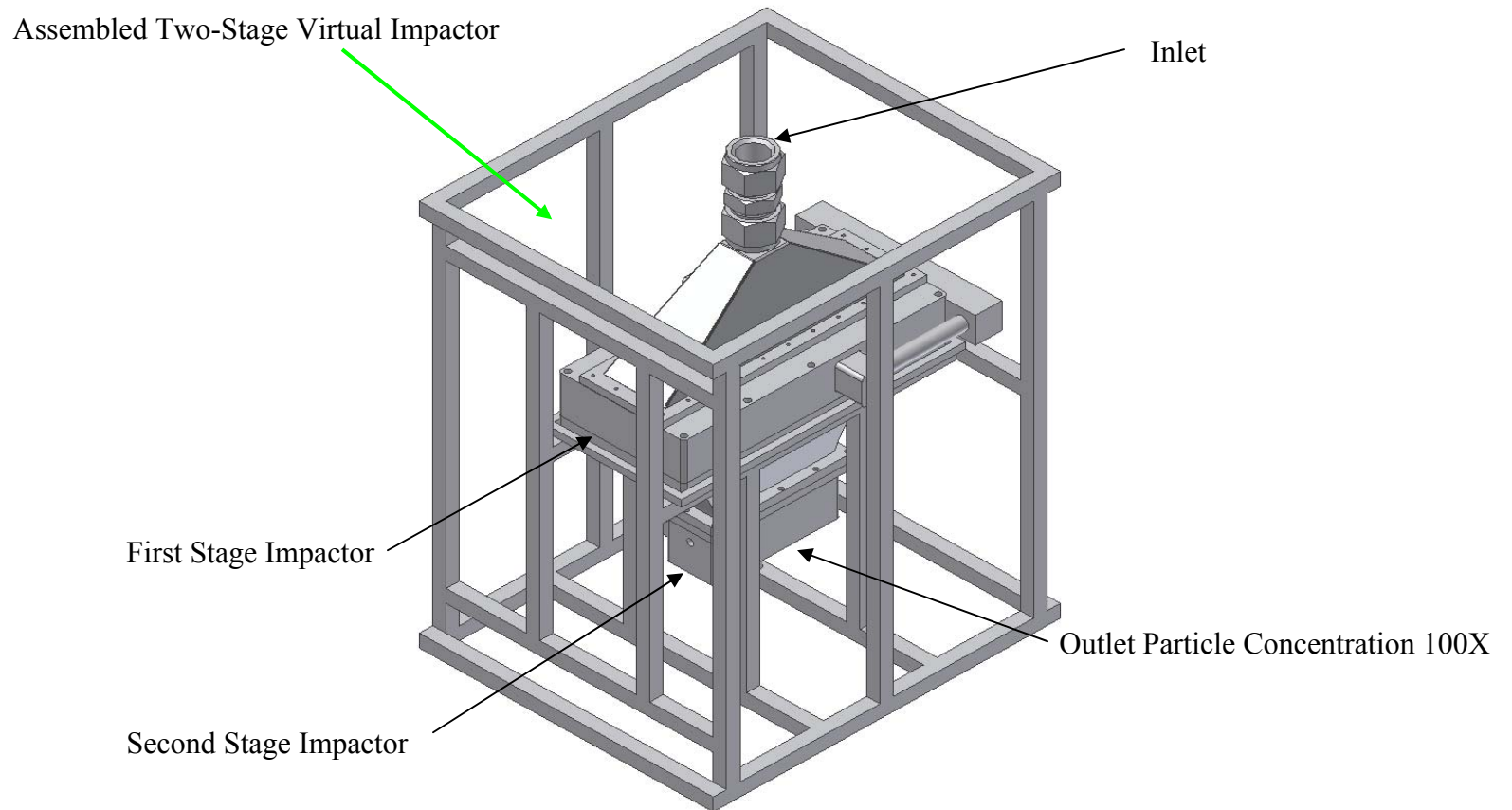


**Figure 4.** CAD drawing of EULSI and second stage impactor.

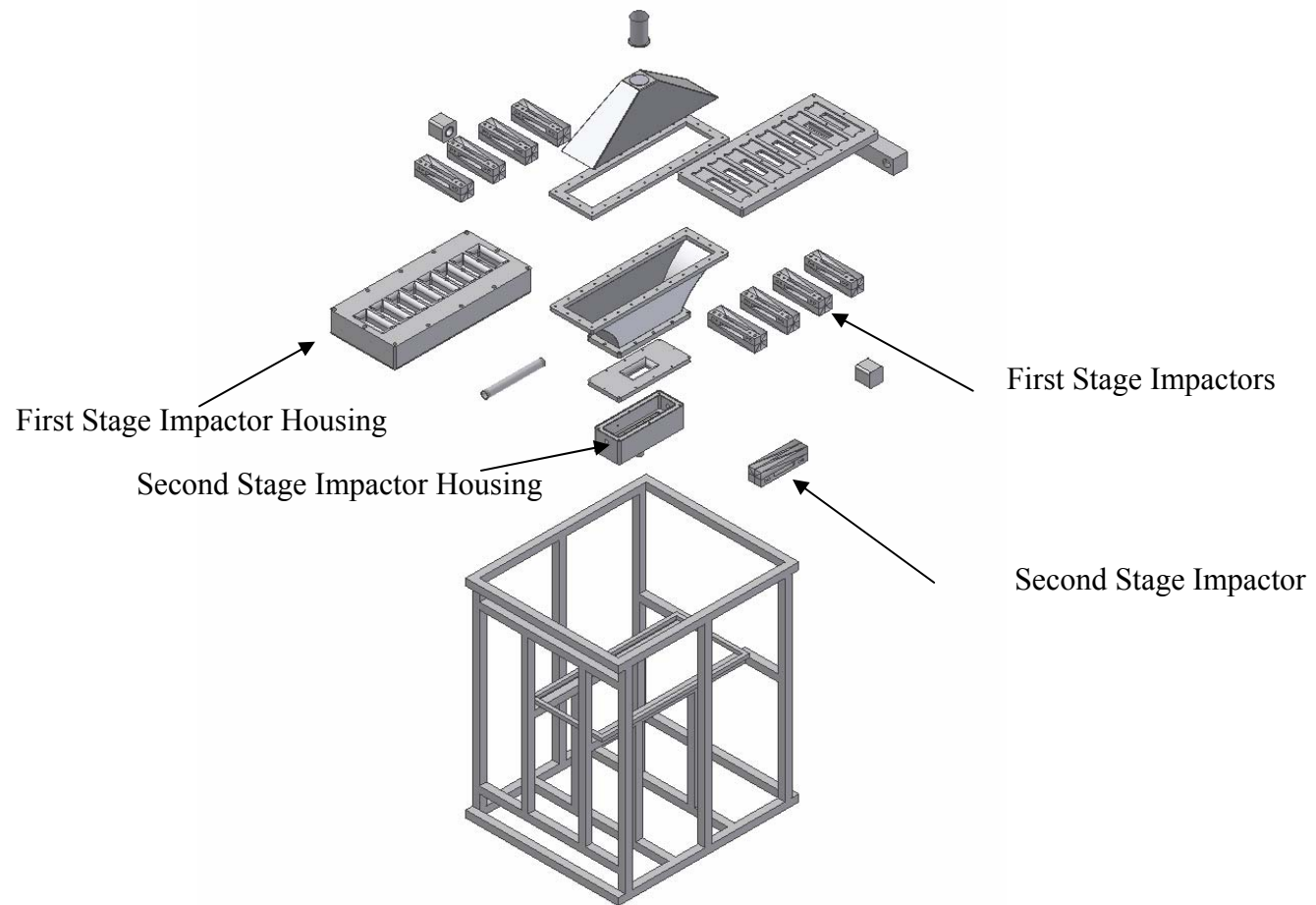


**Figure 5.** Exploded view of two-stage virtual impactor.



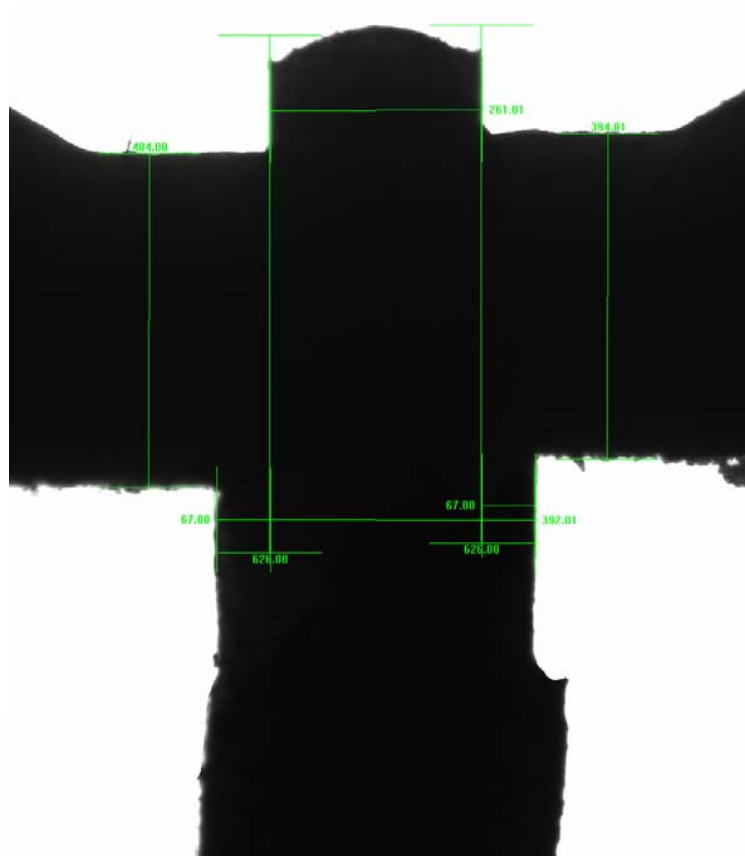


**Figure 6.** Microscopic view of LSVI #20 critical geometry with the two-component putty method.

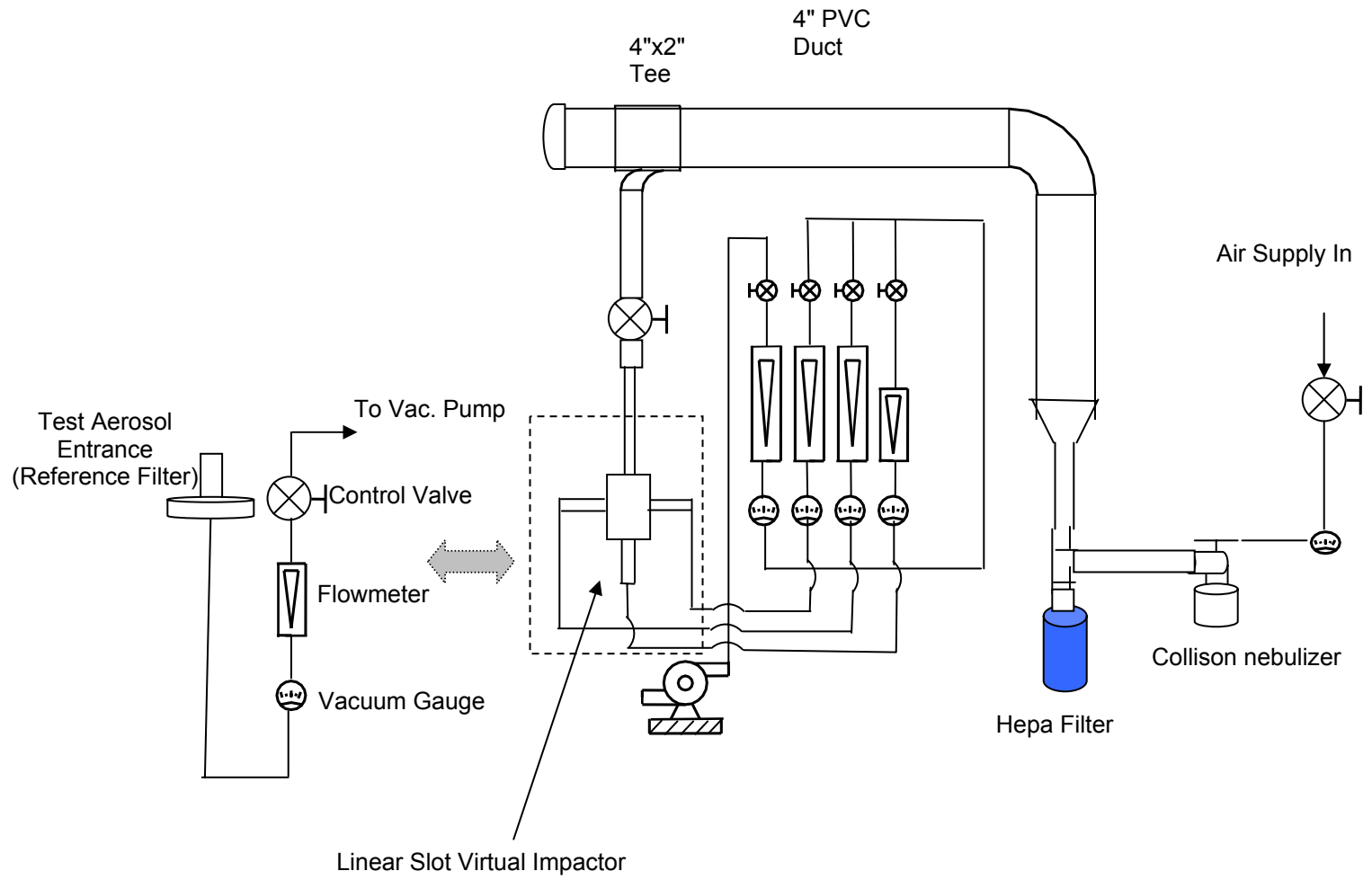


**Figure 7.** Flow transport system for solid particles.

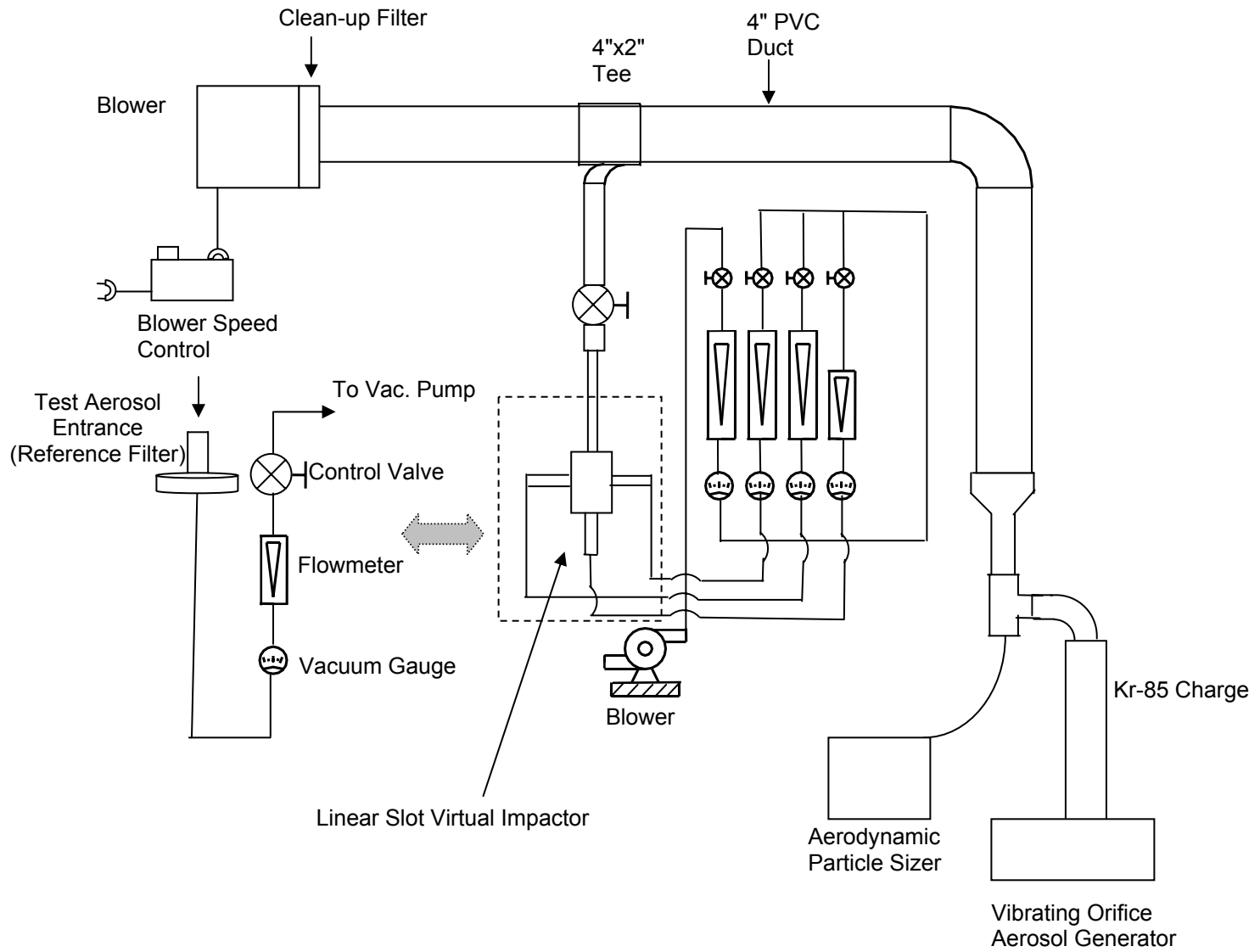


**Figure 8.** Fluid transport system for liquid particles.

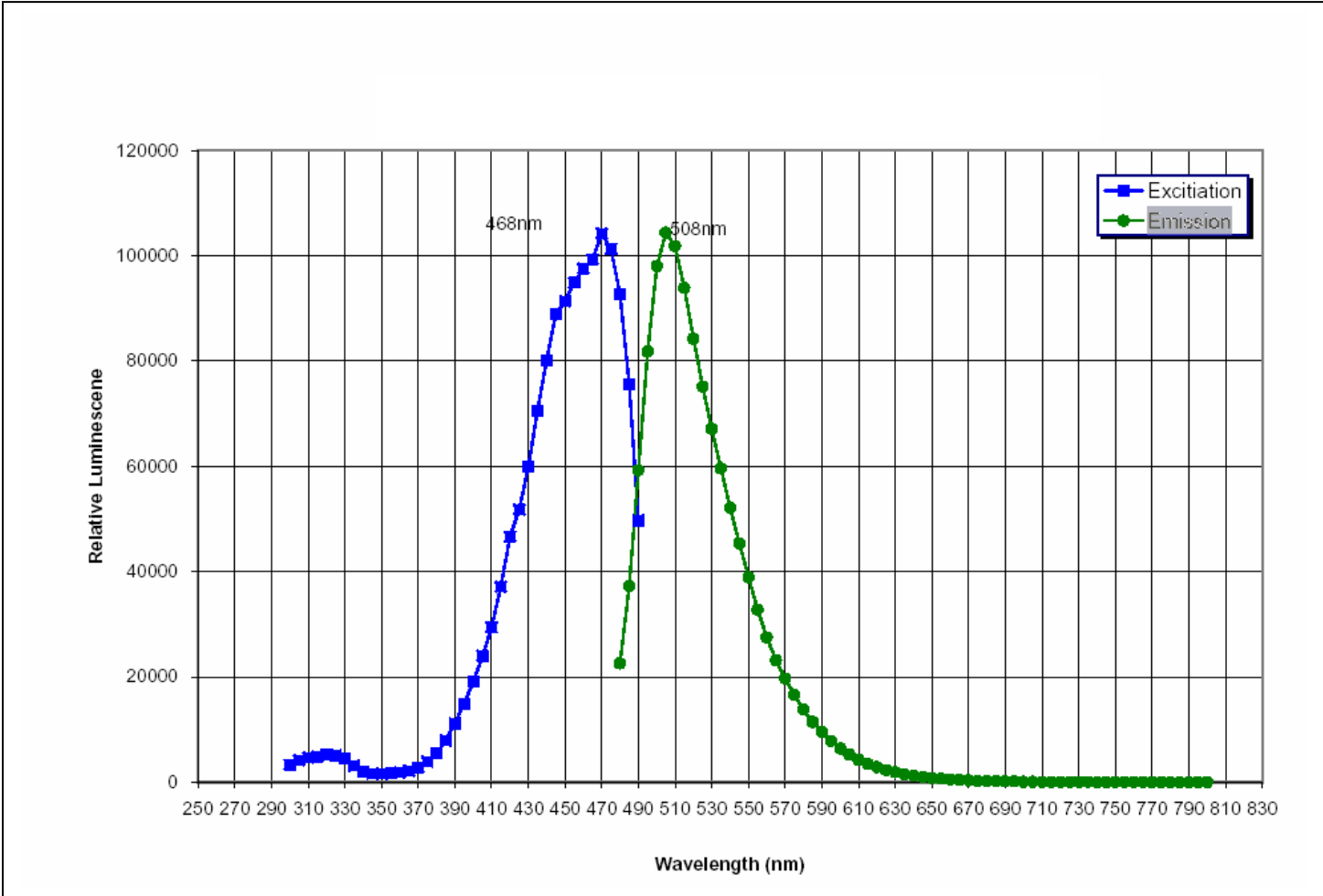
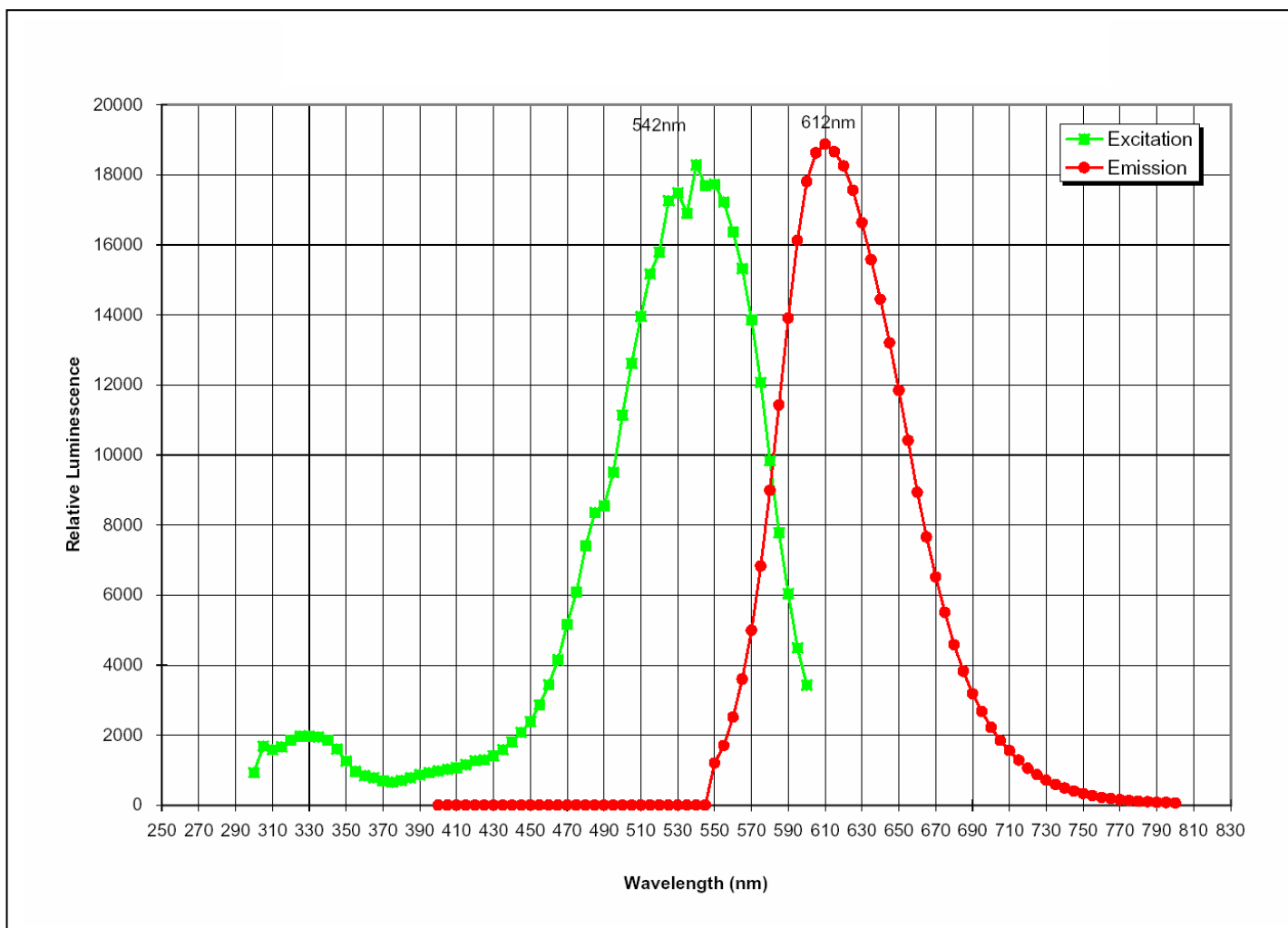
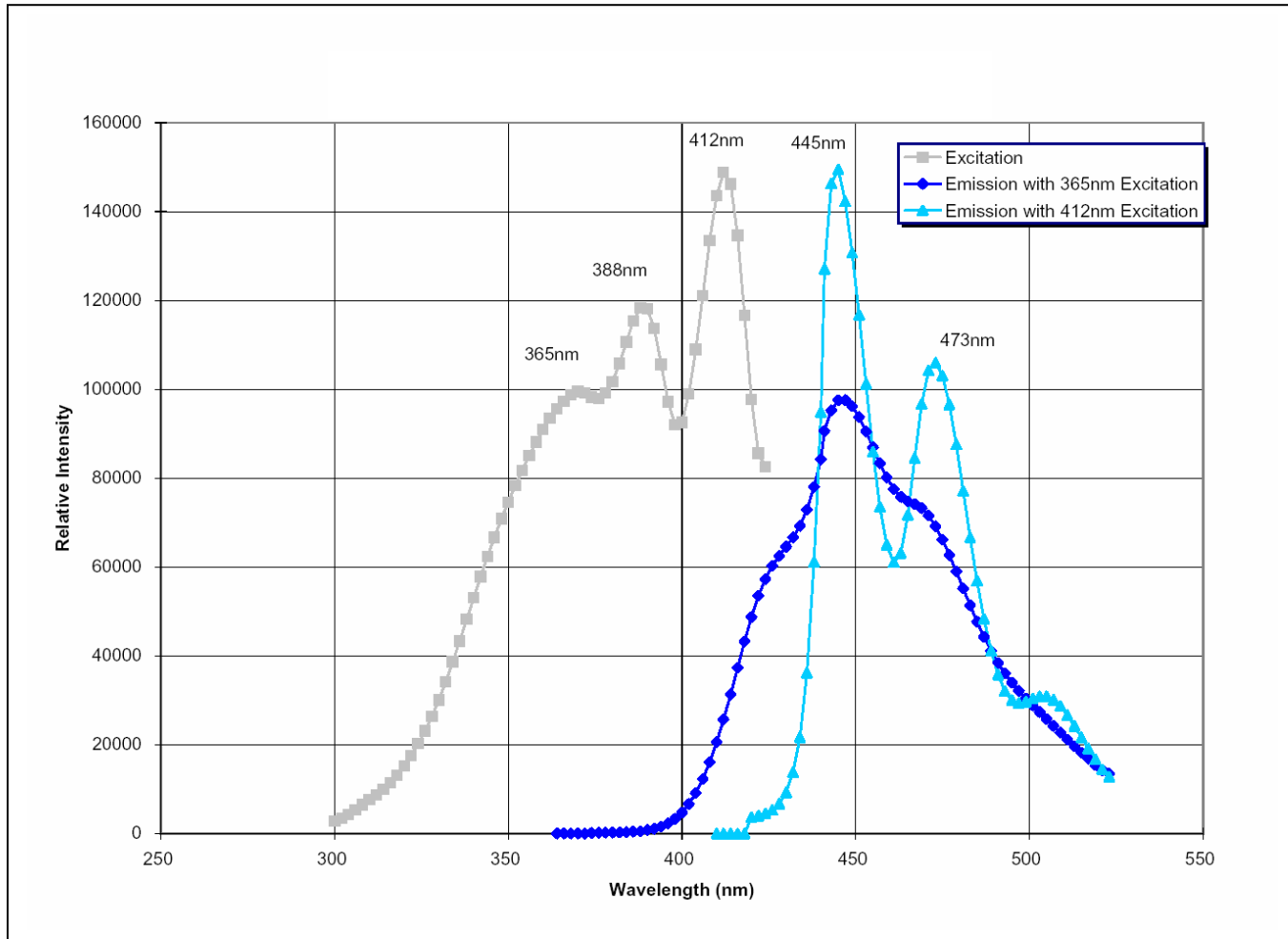


Figure 9. Luminescence vs. wavelength for Duke Scientific green PSL.



**Figure 10.** Luminescence vs. wavelength for Duke Scientific red PSL.



**Figure 11.** Luminescence vs. wavelength for Duke Scientific blue PSL.

**Table 1.** Illumination intensity for blue, green, and red PSL with different filters.

<b>Filter</b>		<b>Color</b>	<b>Percent of Excited Particles</b>	<b>Background concentration</b>
<b>Excitation</b>	<b>Emission</b>			
NB 360	NB 440	Blue	98.24%	0.89%
NB 360	NB 440	Green	5.59%	0.89%
NB 360	NB 440	Red	5.82%	0.89%
NB 460	NB 490	Blue	0.33%	0.22%
NB 460	NB 490	Green	98.56%	0.22%
NB 460	NB 490	Red	1.10%	0.22%
NB 540	NB 590	Blue	0.87%	0.58%
NB 540	NB 590	Green	0.94%	0.58%
NB 540	NB 590	Red	96.99%	0.58%

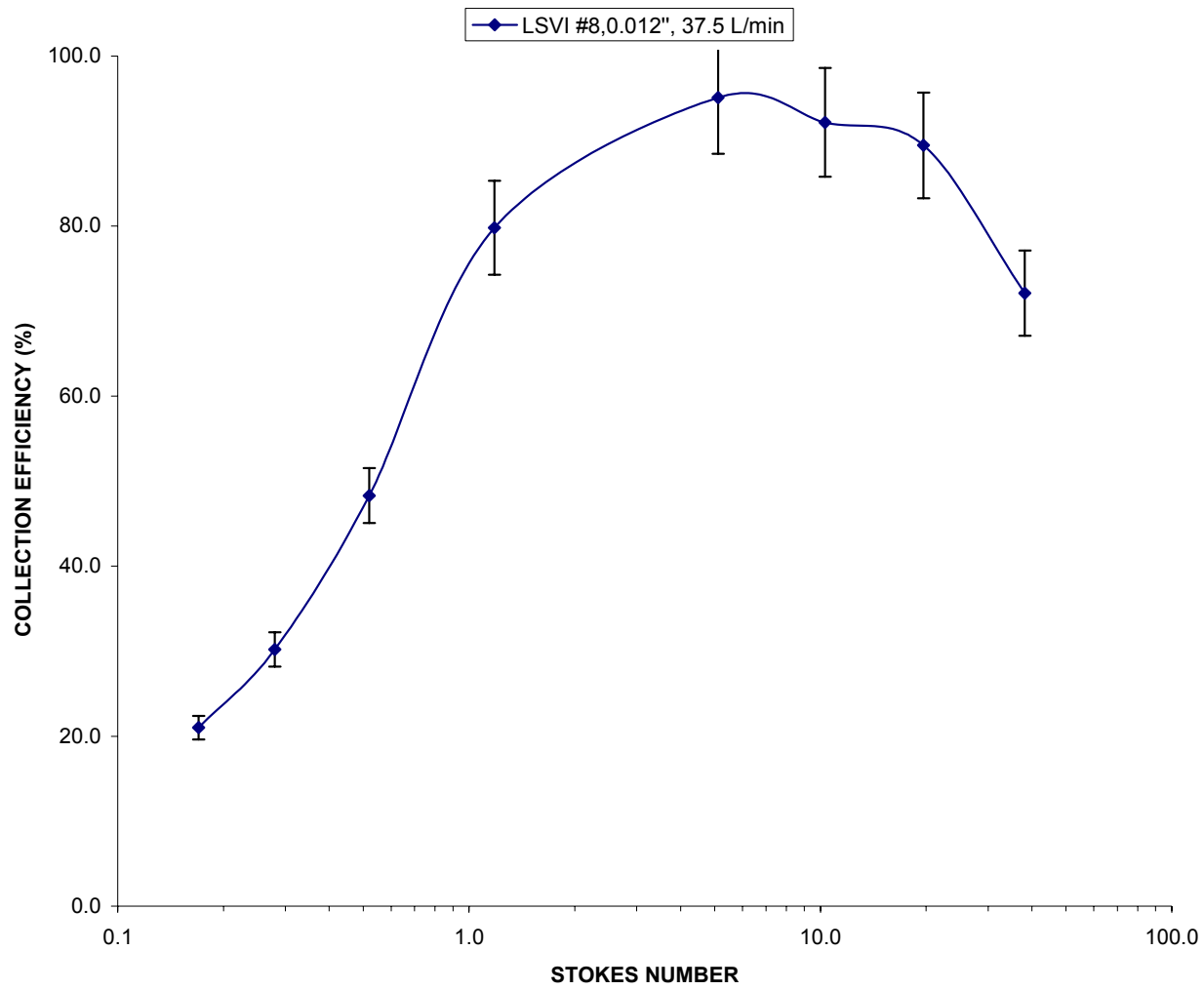


**Figure 12.** Minor flow collection efficiency vs. Stk for LSVI #8 at 37.5 L/min.





**Figure 13.** Outlet view of the EUSLI system.

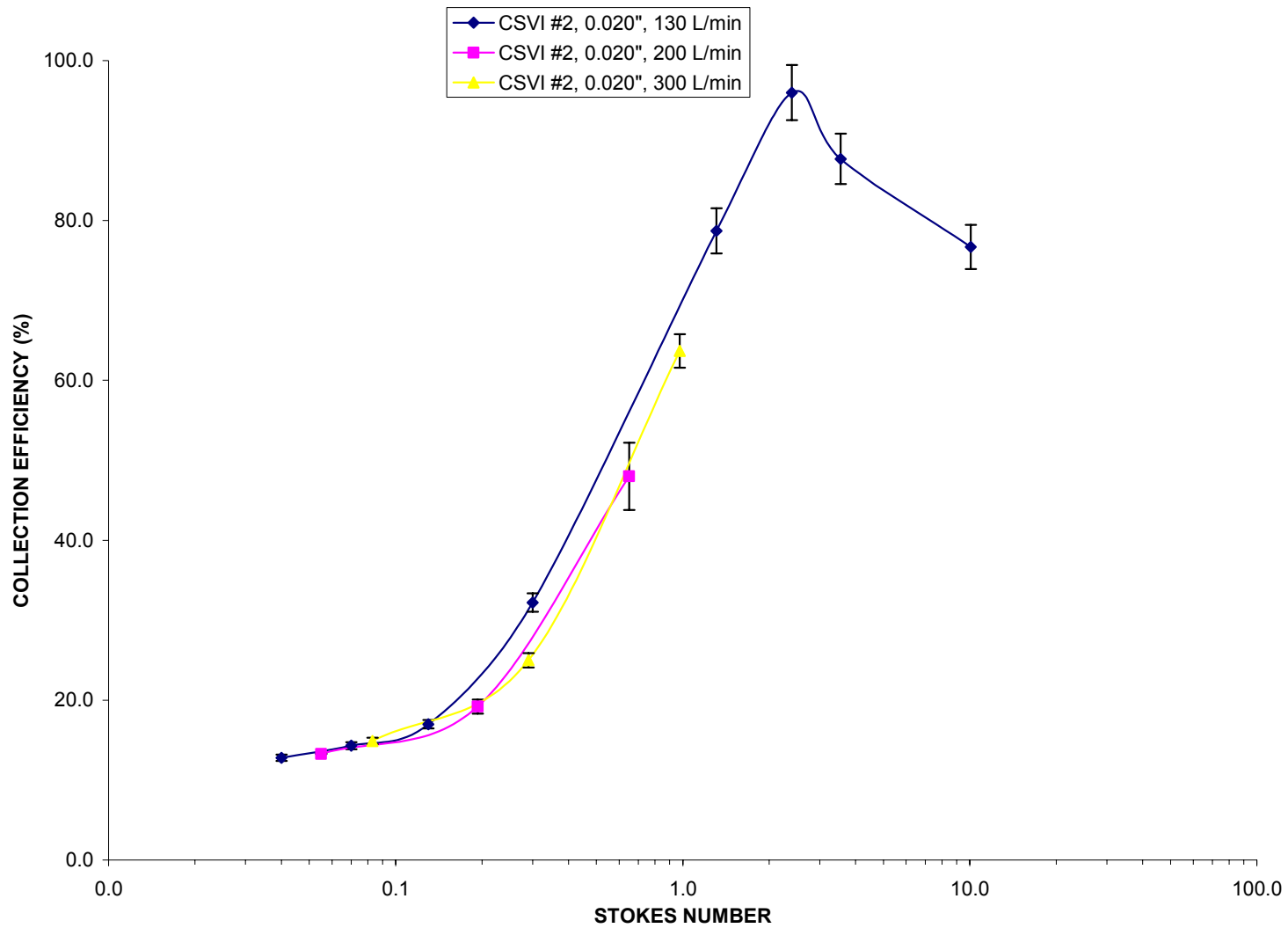


**Figure 14.** Minor flow collection efficiency vs. Stk for CSVI #2 with sound suppression device.

**Table 2.** Critical dimensions for EULSI units.

Impactor	Accelerator Width (1/1000")	Receiver Width (1/1000")	Offset Width (1/1000")
8	12.30	17.92	0.25
9	12.93	18.73	0.18
10	12.83	19.92	0.21
11	12.98	19.85	0.22
12	13.65	19.77	0.20
13	13.84	19.45	0.54
14	12.72	19.52	0.17
15	13.77	19.24	0.21
16	13.17	19.33	0.27
17	13.36	19.80	0.17
Average Width	13.18	19.52	0.20

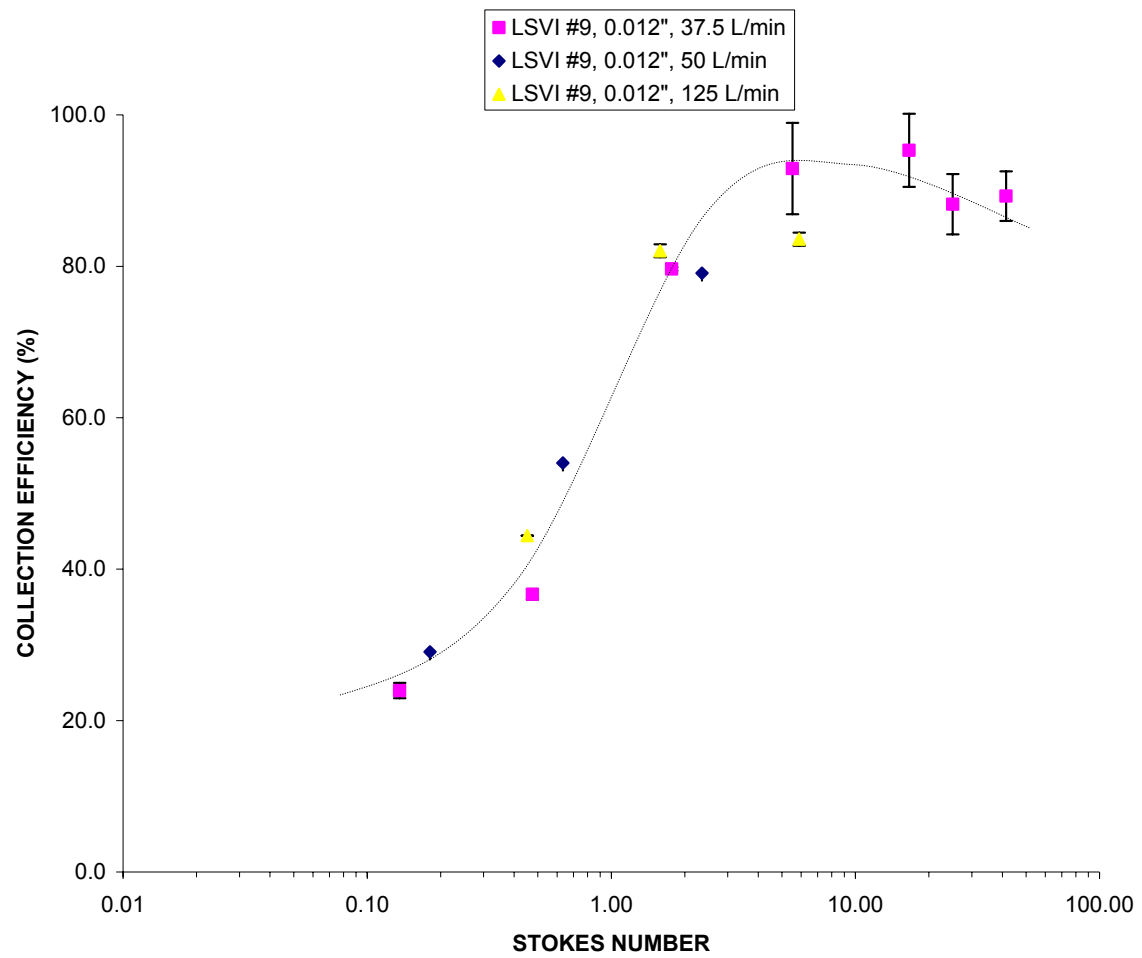


**Figure 15.** Minor flow collection efficiency vs. Stk for LSVI #9 at the tested flow rates.

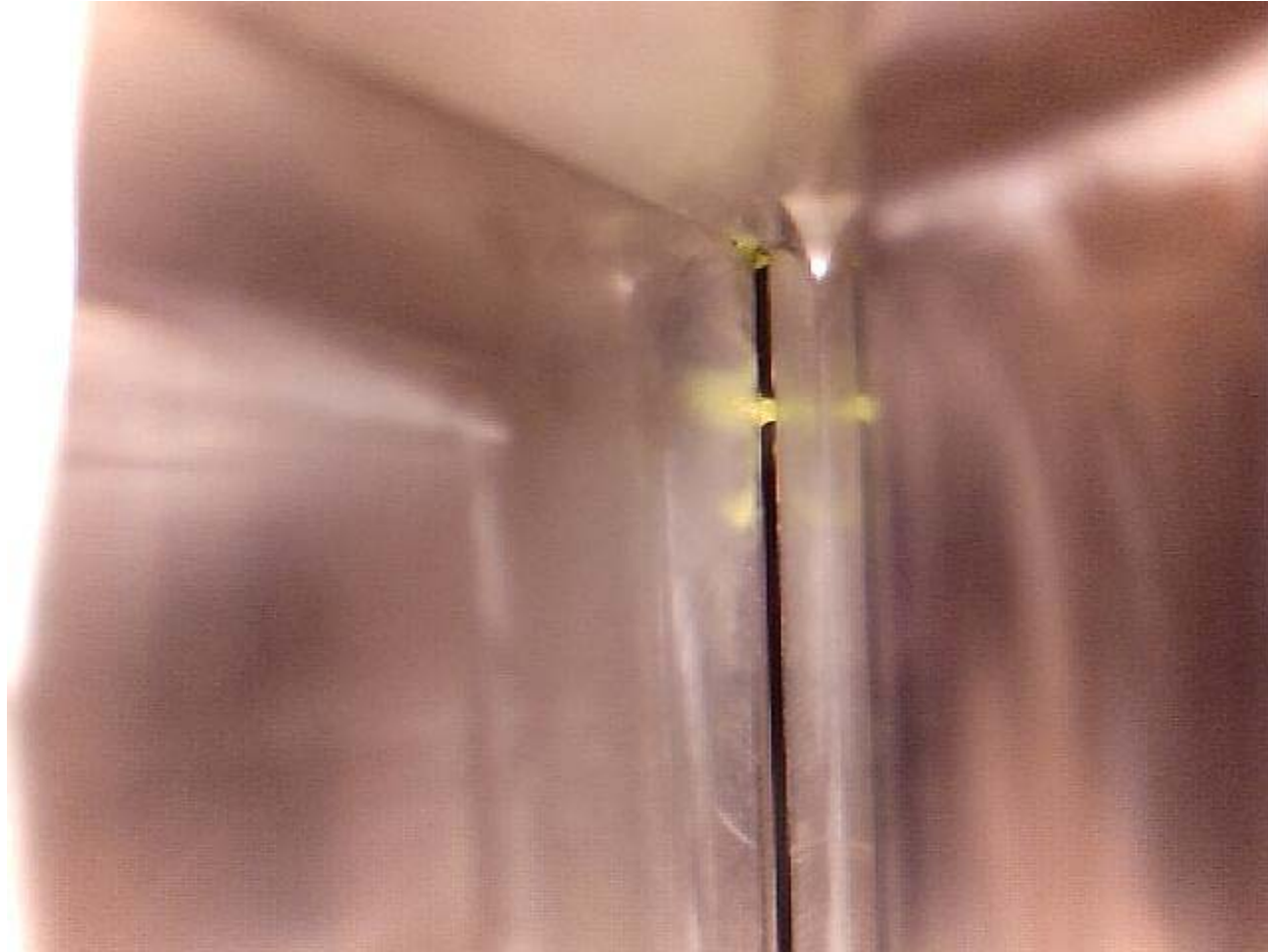


**Figure 16.** Deposition on the throat end of LSVI #9.

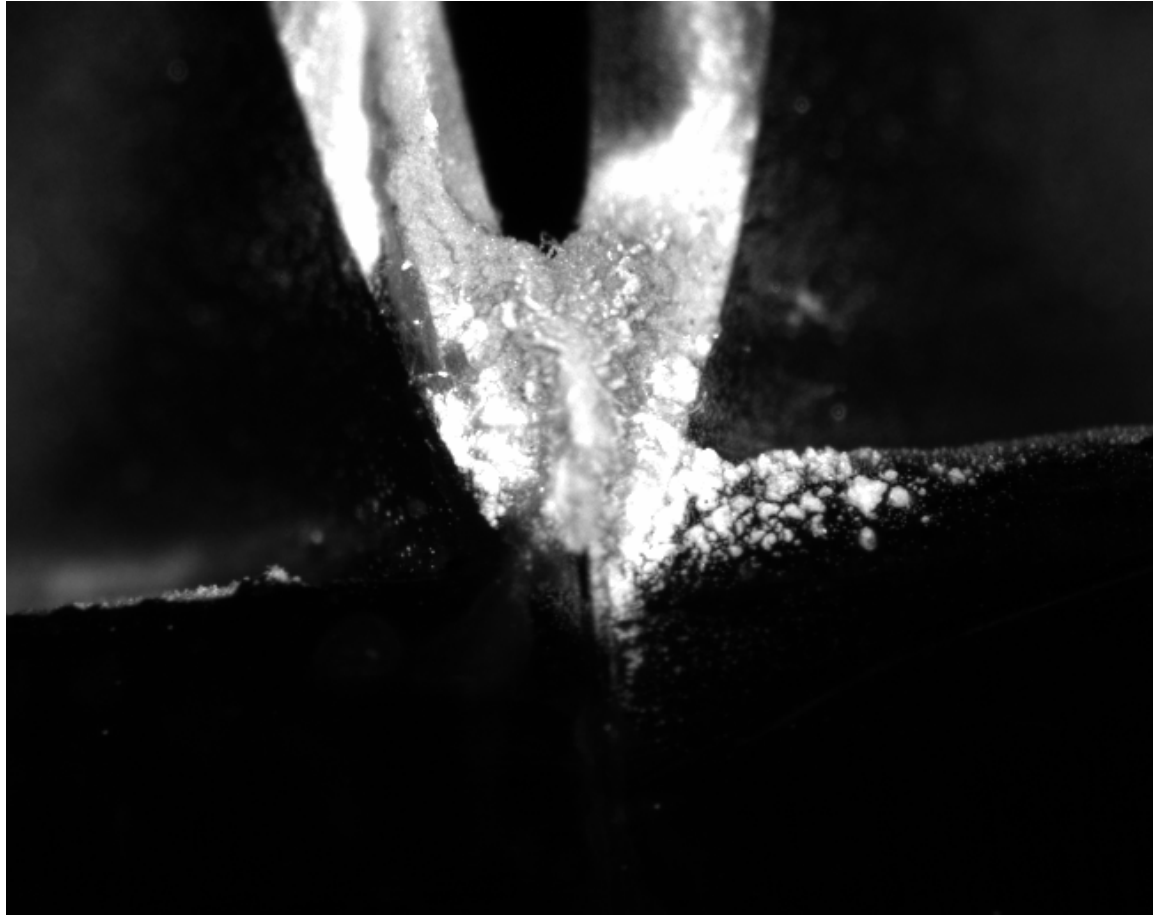


**Figure 17.** 2  $\mu\text{m}$  solid particle deposition for LSVI #9 at 125 L/min.

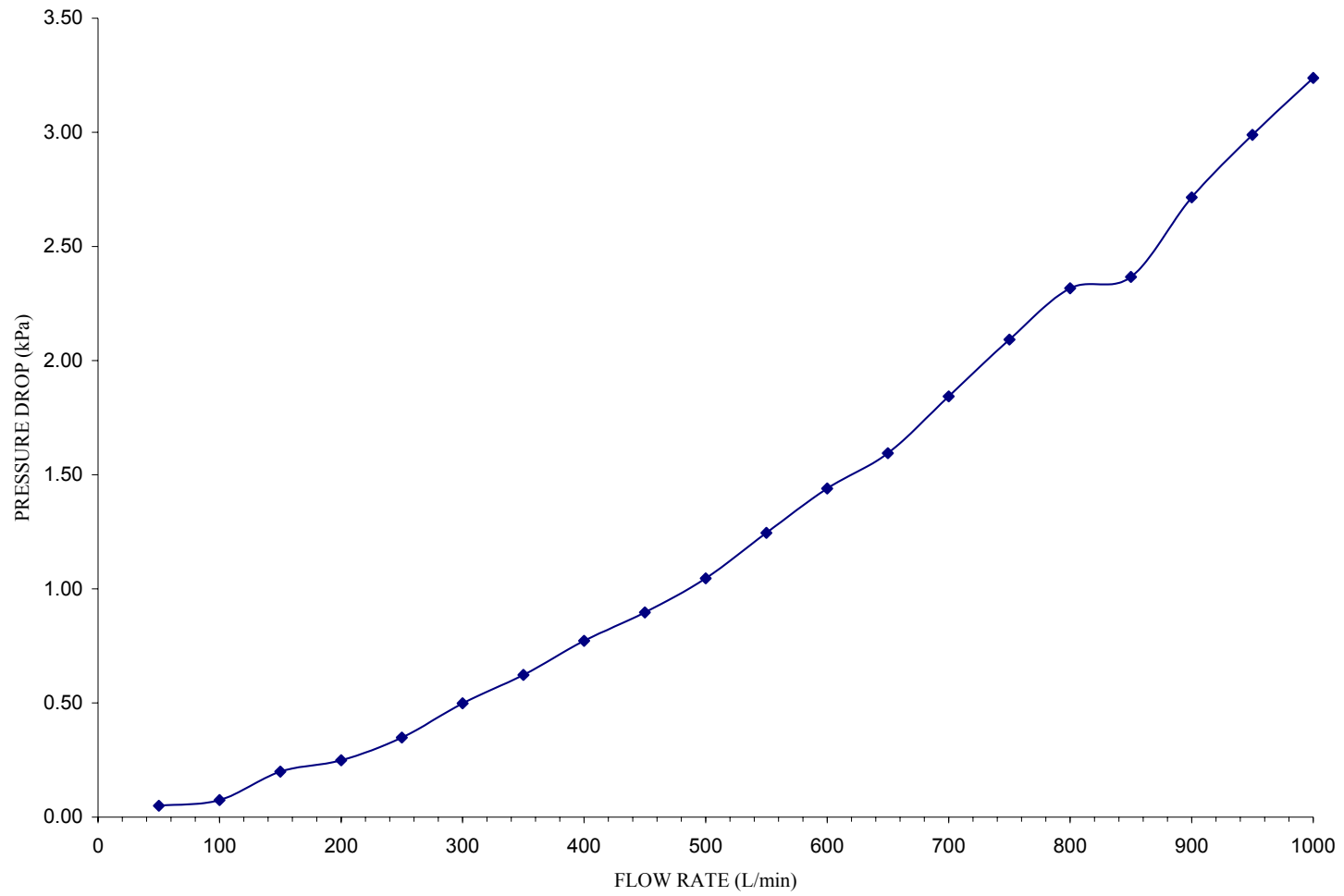


**Figure 18.** Pressure drop inside the EUSLI system at various flow rates.

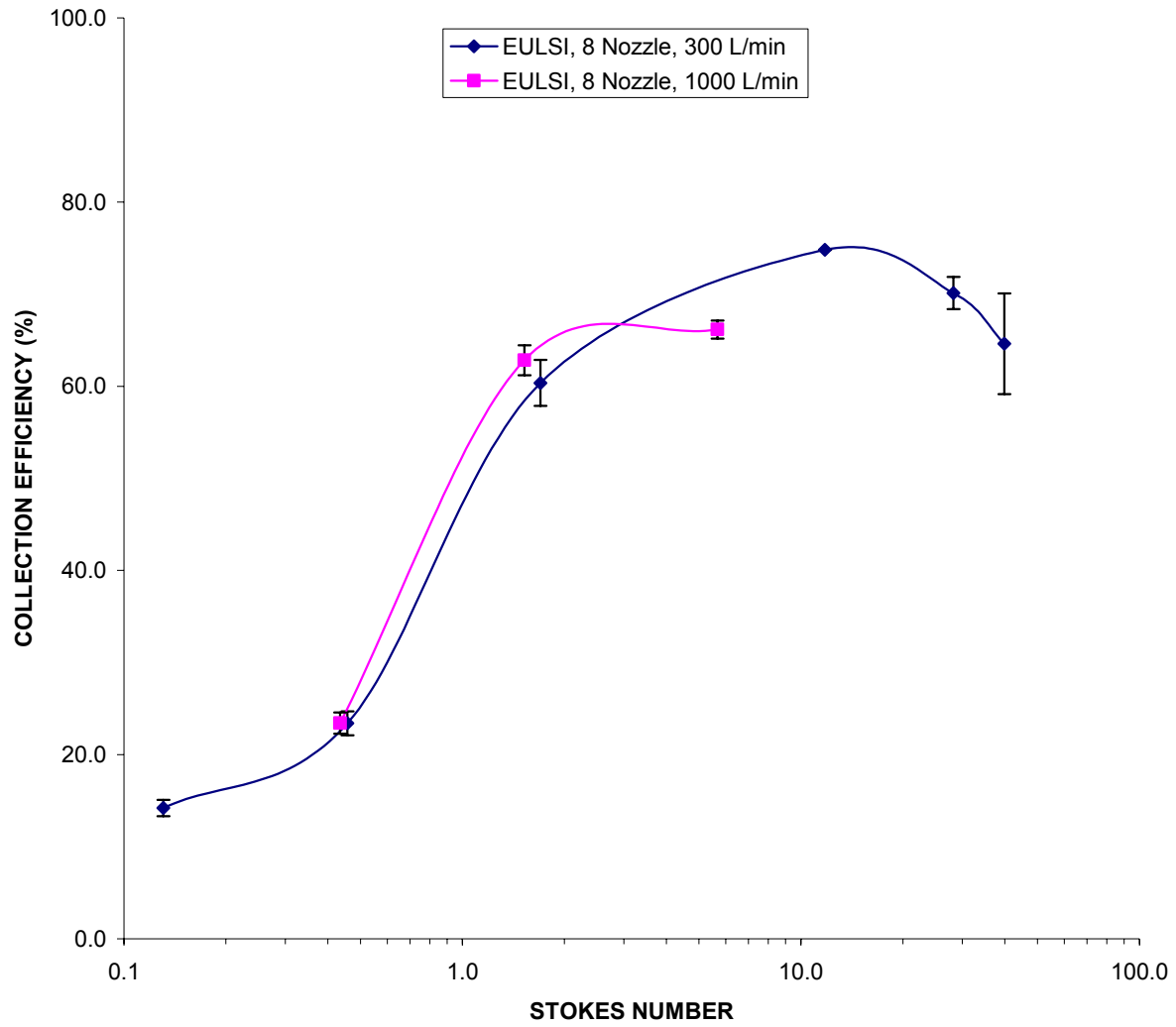


**Figure 19.** Minor flow collection efficiency vs. Stk for EULSI for tested flow rates.



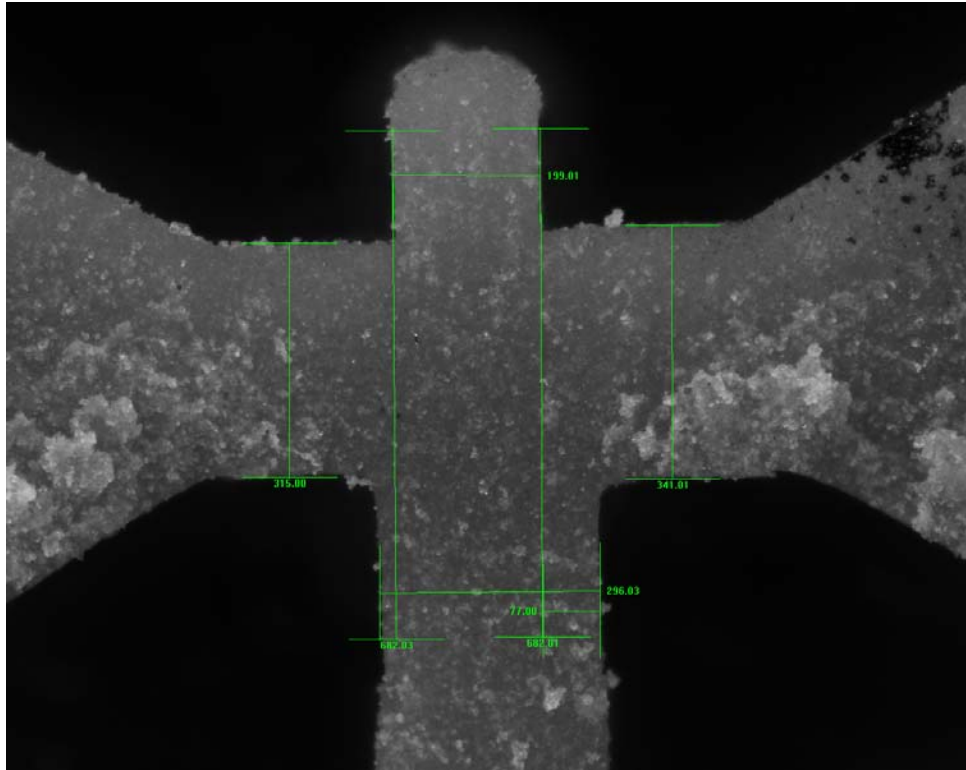


**Figure 20.** Microscopic view of LSVI #18 critical geometry.

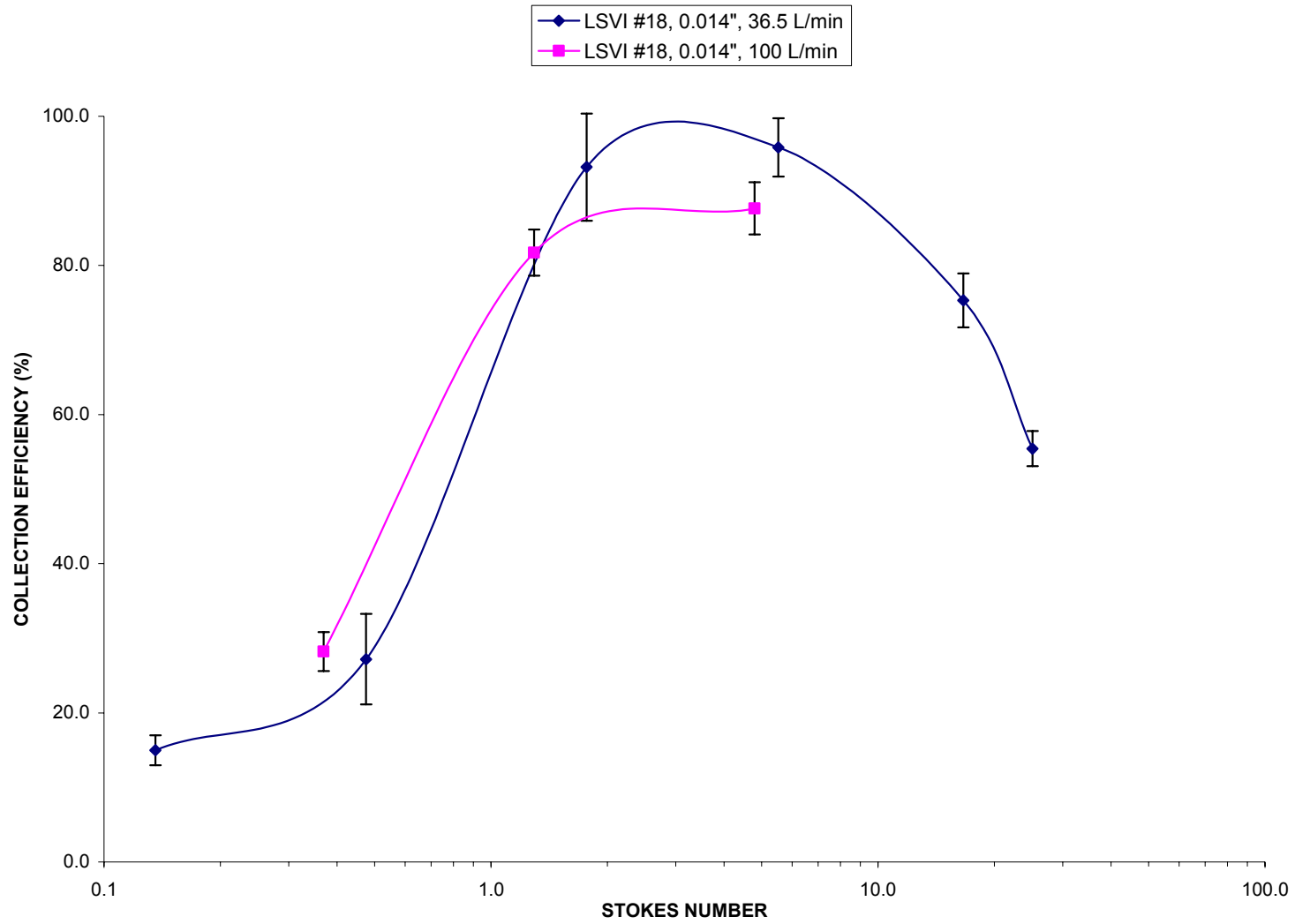


**Figure 21.** Minor flow collection efficiency vs. Stk for LSVI #18 at the tested flow rates.

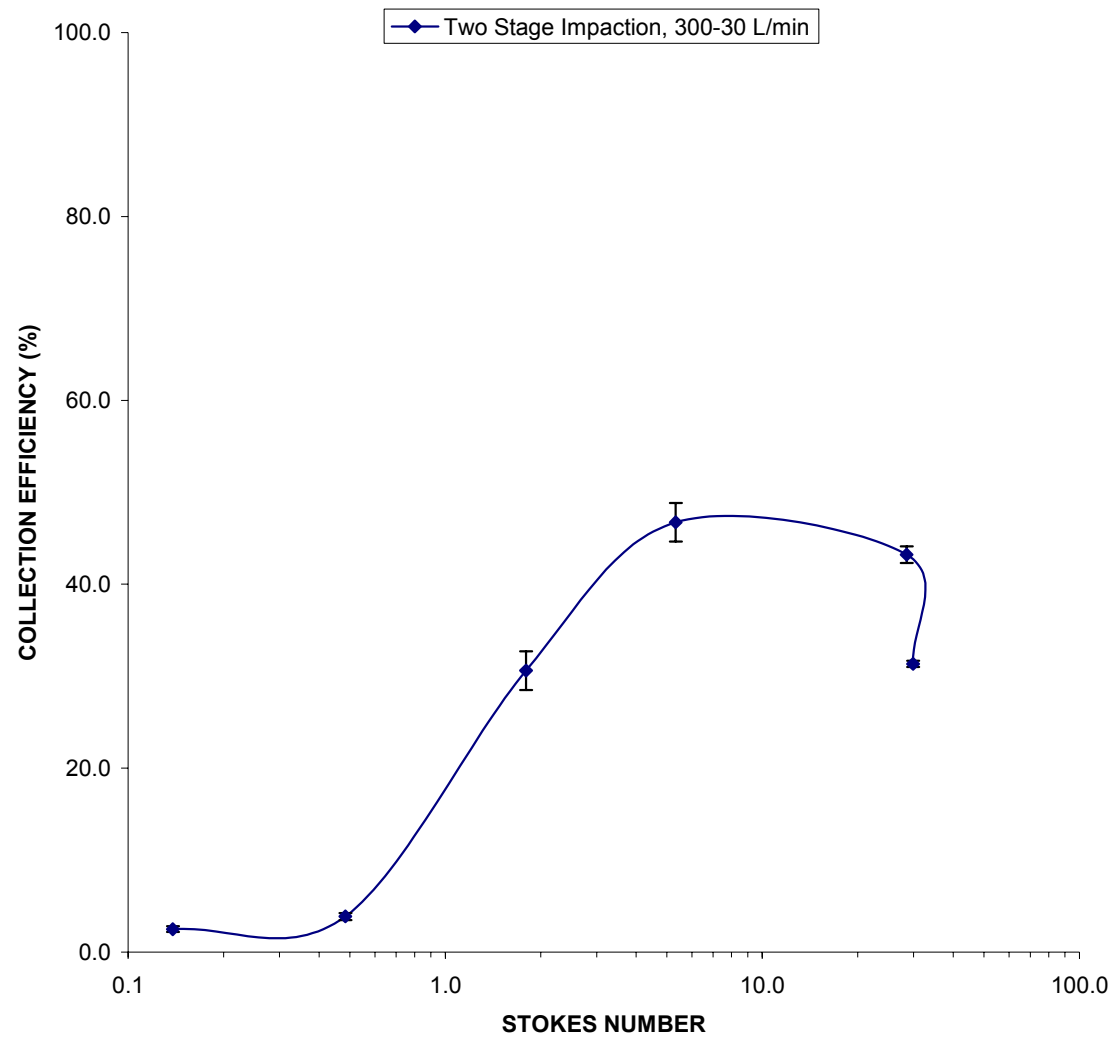


**Figure 22.** Minor flow collection efficiency vs. Stk for two-stage impaction of EULSI

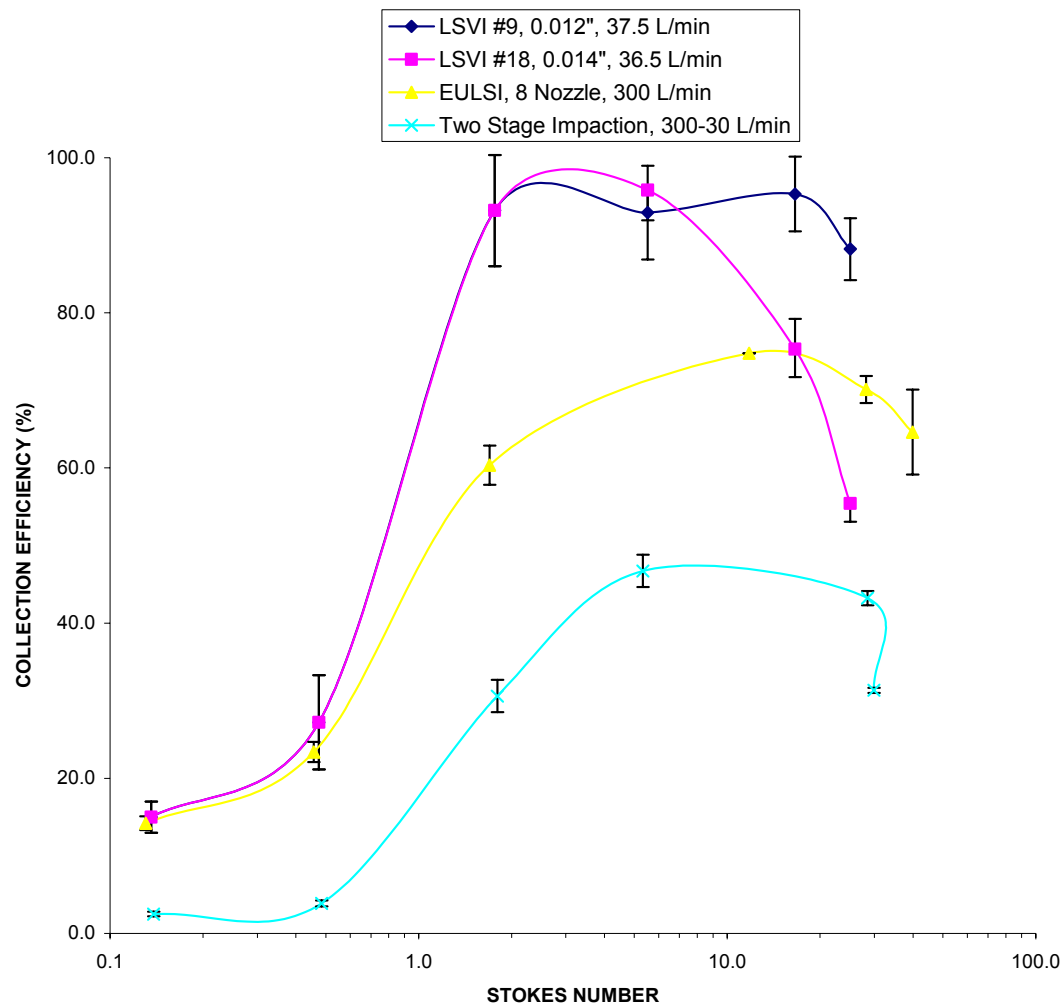


**Figure 23.** Minor flow collection efficiency vs. Stk for multi-nozzle two-stage impactation at 300 L/min.

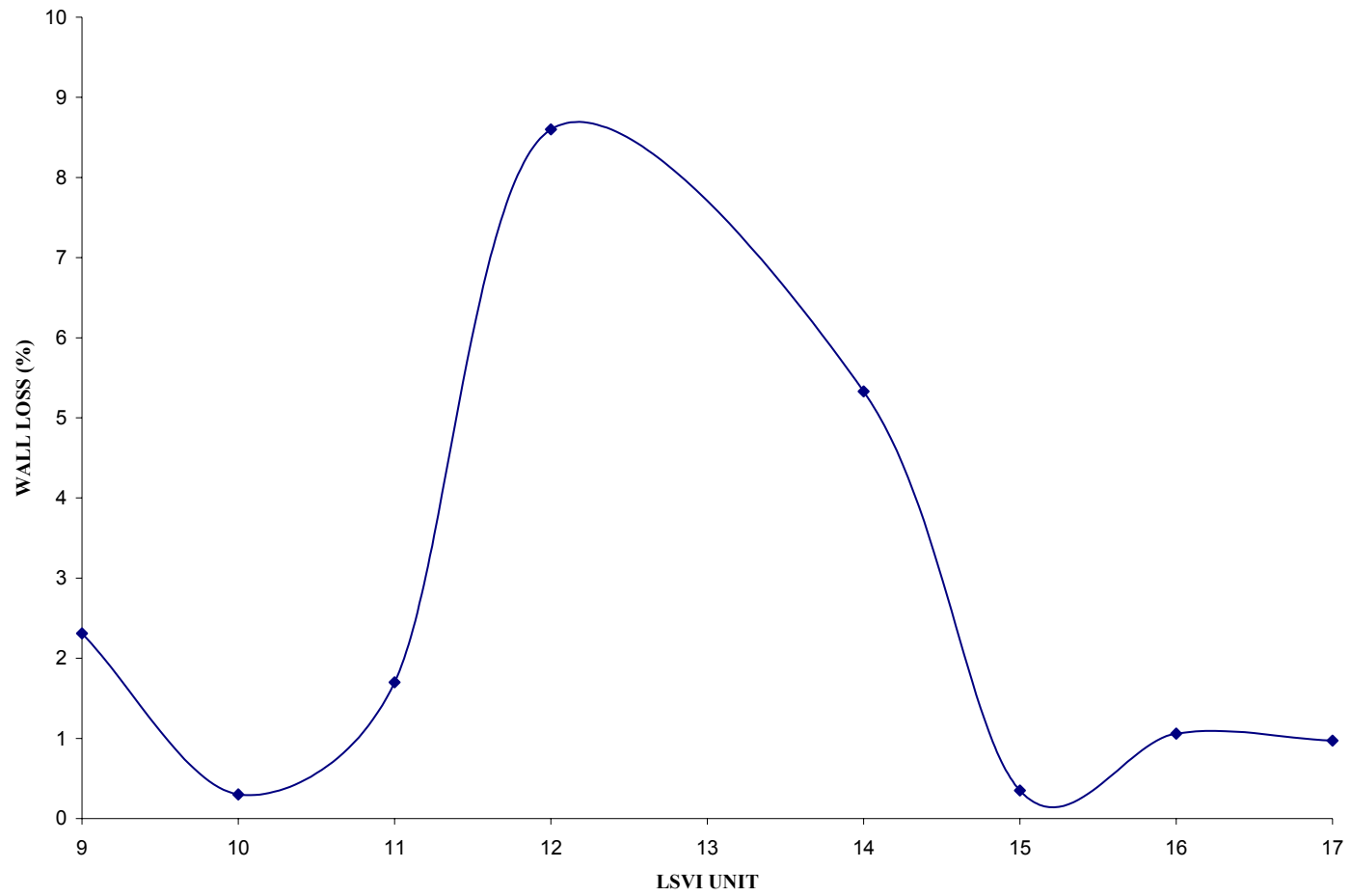


**Figure 24.** Plot of wall losses for each impactor inside EULSI.

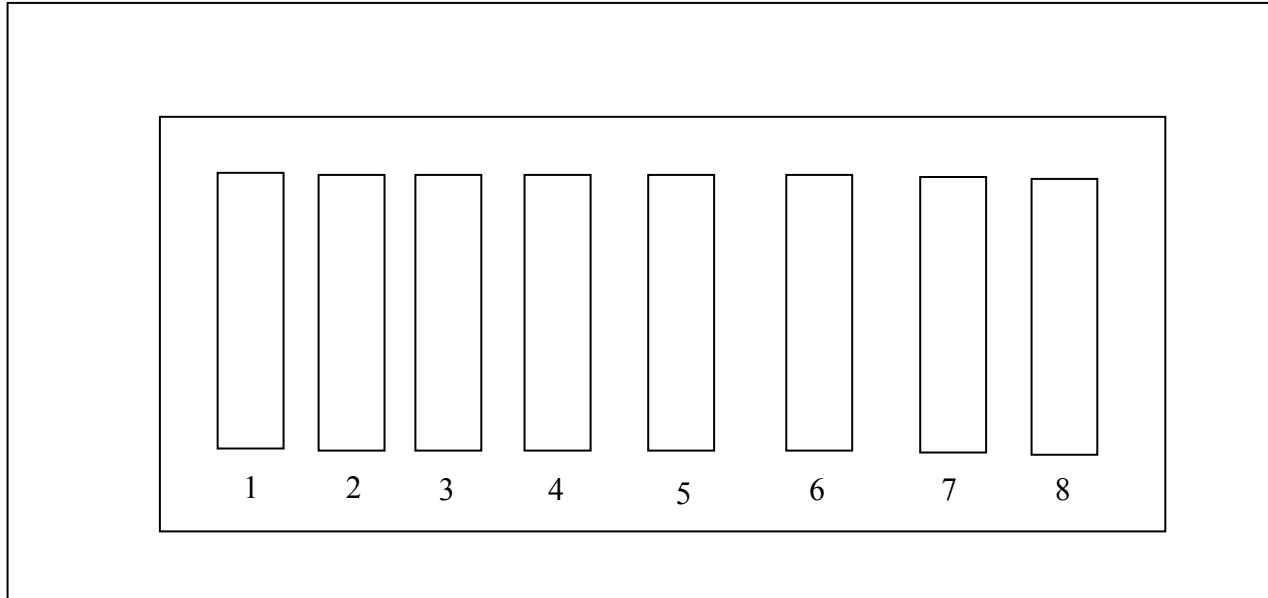


**Figure 25.** EULSI diagram for labeling the various LSVI arrangements.

**Table 3.** List of various models used in LSVI arrangements.

Model	Positions
A.	4
B.	4,5
C.	4,6
D.	3,4,5
E.	3,4,6,8
F.	3,4,6,7,8
G.	1,3,4,6,7,8
H.	1,3,4,5,6,7,8

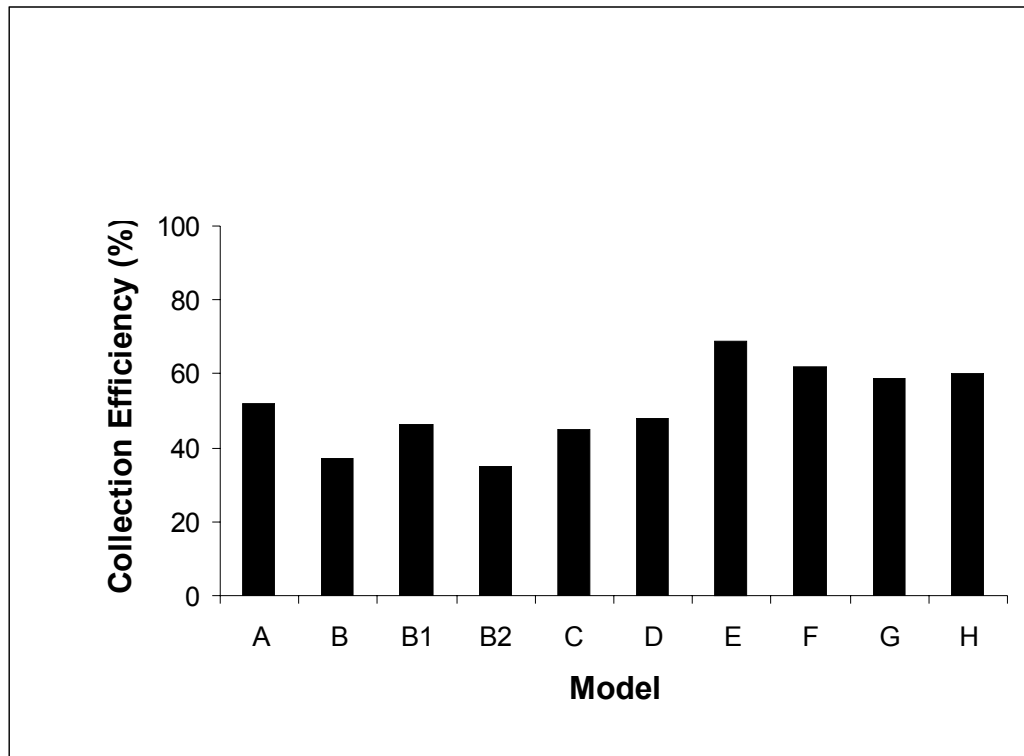


**Figure 26.** Minor flow collection efficiency of 2 μm particles for various LSVI arrangements.

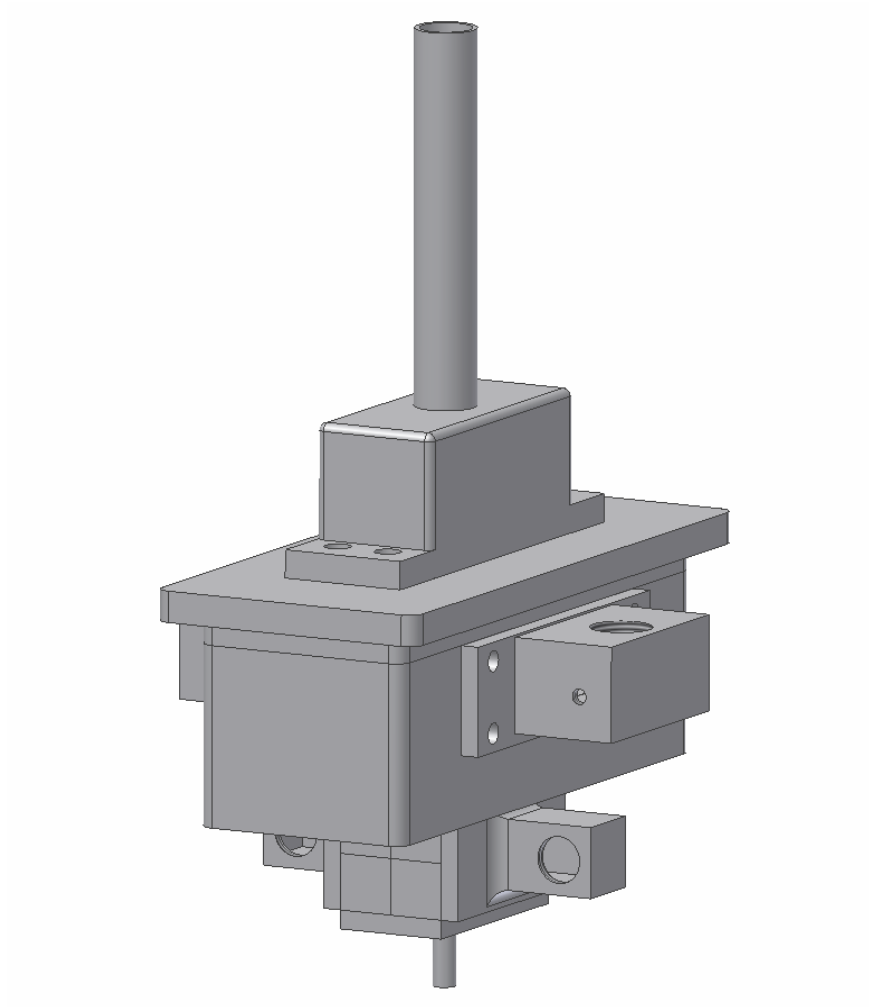


**Figure 27.** CAD view of 100 L/min two-stage impactor.



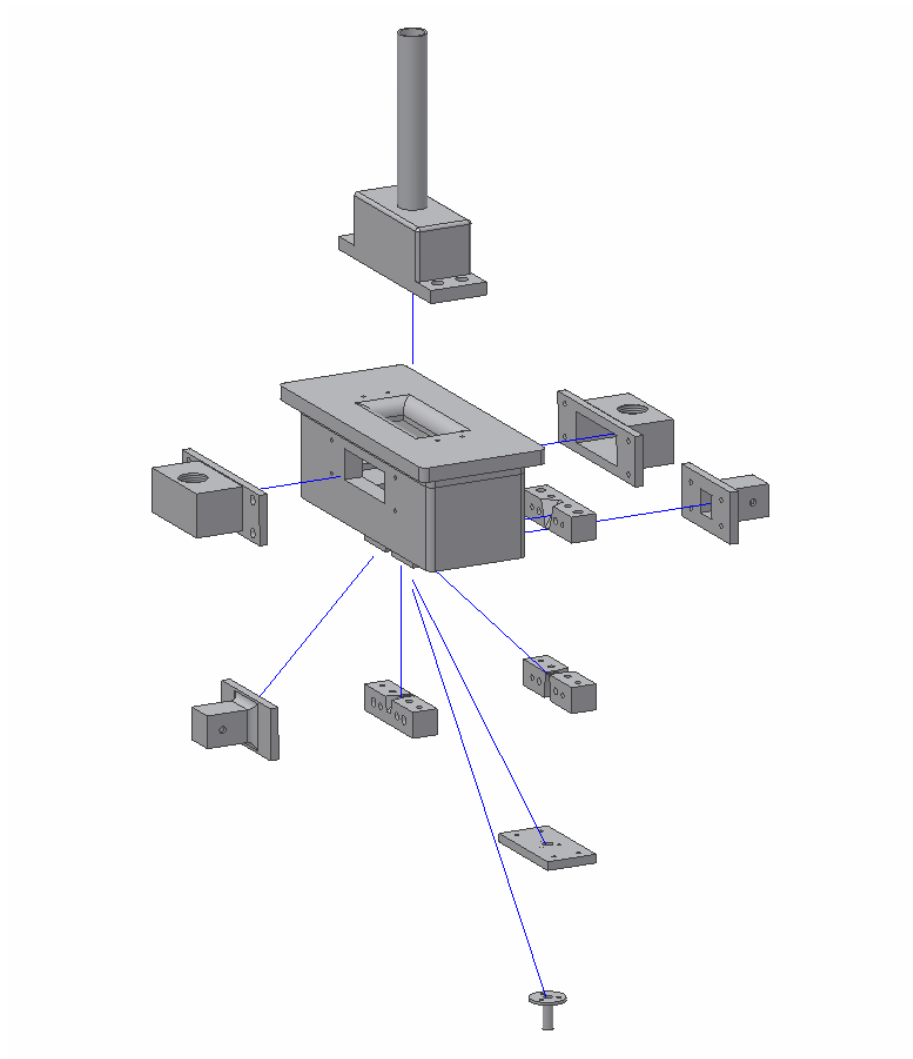


**Figure 28.** Exploded CAD view of 100 L/min two-stage impactor.

**Table 4.** Critical dimensions for LSVI #13, #18, and #20.

<b>LSVI #13</b>		
Acceleration nozzle width:	0.4318 mm	(0.017")
Receiver nozzle width:	0.6350 mm	(0.025")
Average Misalignment:	0.003 mm	(0.0001)"
Slot length:	87.312 mm	(3.4375")
<b>LSVI #18</b>		
Acceleration nozzle width:	0.3347 mm	(0.01318")
Receiver nozzle width:	0.4958 mm	(0.01952")
Misalignment	0.013 mm	(0.0005")
Slot length:	87.312 mm	(3.4375")
<b>LSVI #20</b>		
Acceleration nozzle width:	0.4318 mm	(0.017")
Receiver nozzle width:	0.6350 mm	(0.025")
Average misalignment:	0.005 mm	(0.0002)"
Slot length:	8.7312 mm	(3.4375")

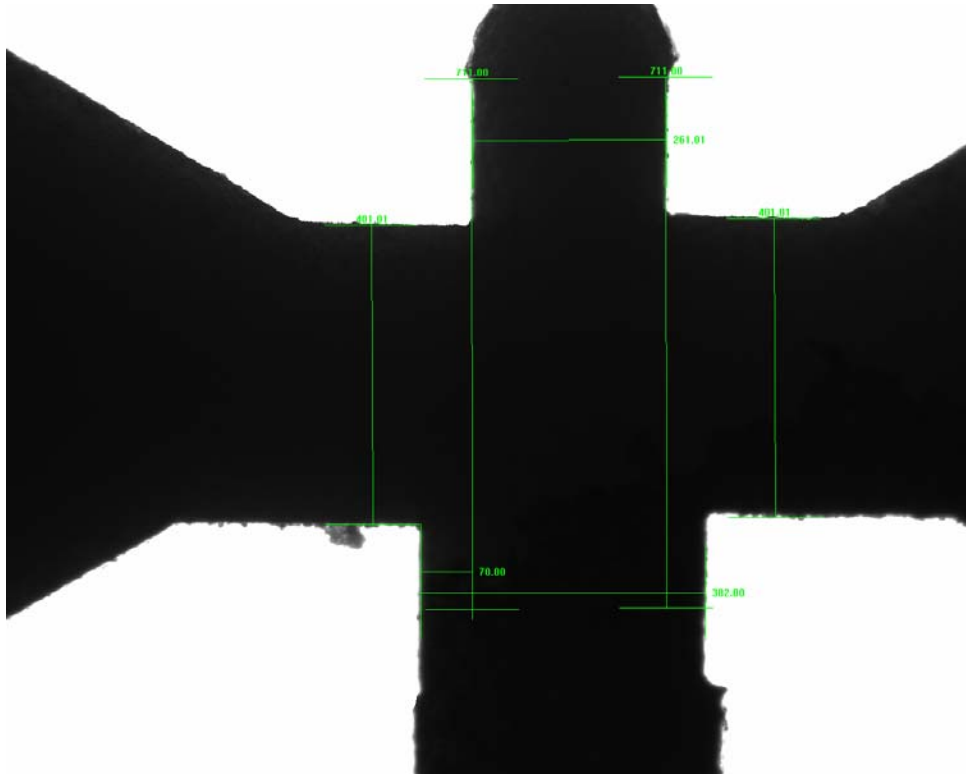


**Figure 29.** Microscopic view of LSVI #13 critical geometry.

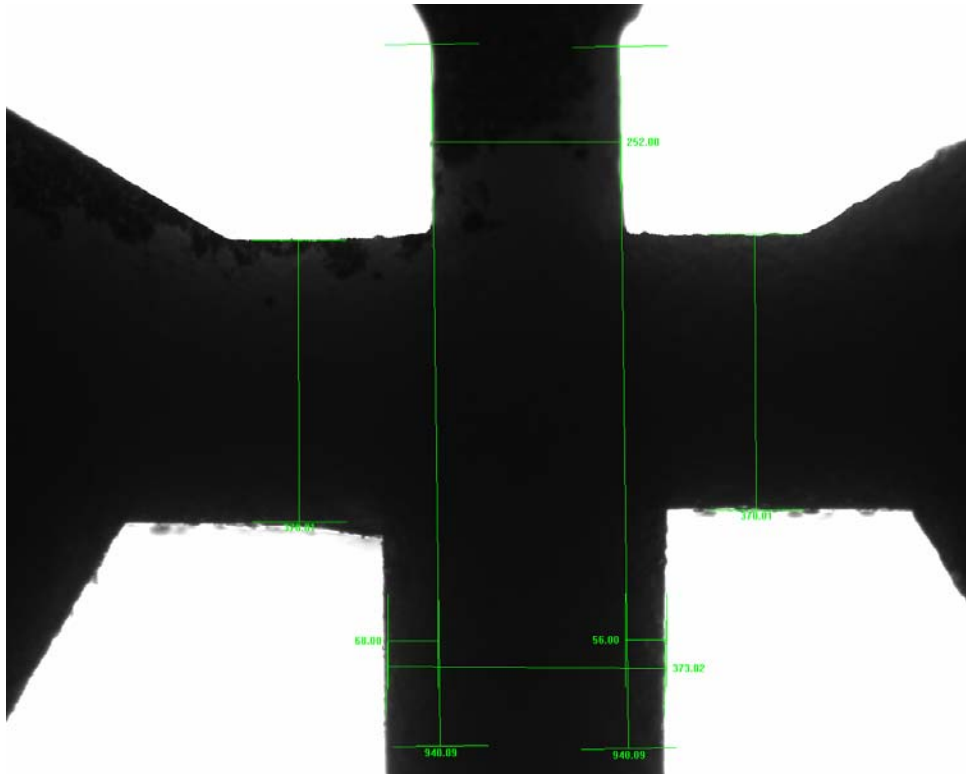


**Figure 30.** Microscopic view of LSVI #20 critical geometry.



**Figure 31.** View of accelerator for second stage impactor.



**Figure 32.** Aerosol transport fixtures for second stage impactor.

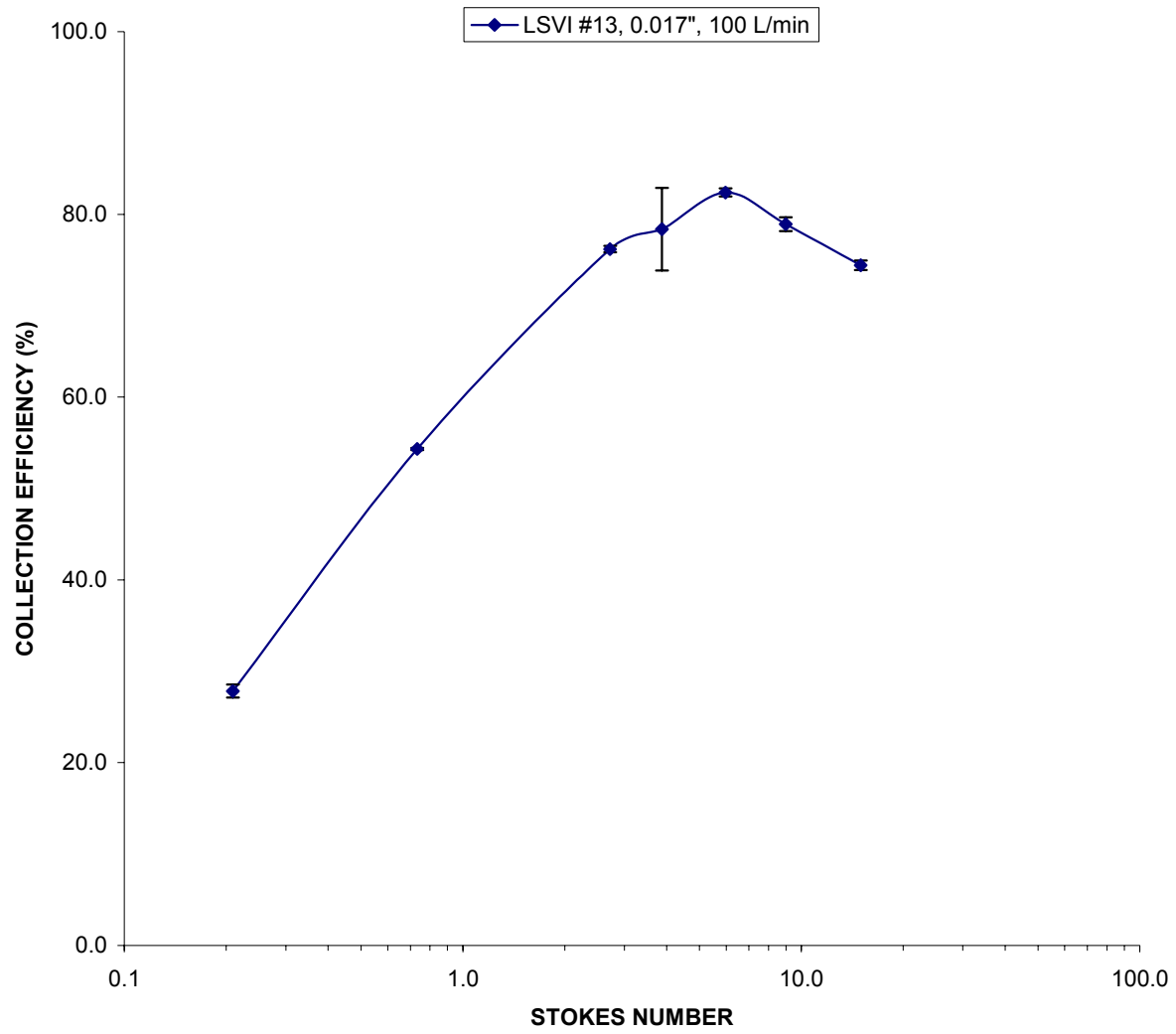


**Figure 33.** Minor flow collection efficiency vs. Stk for LSVI #13 at 100 L/min.

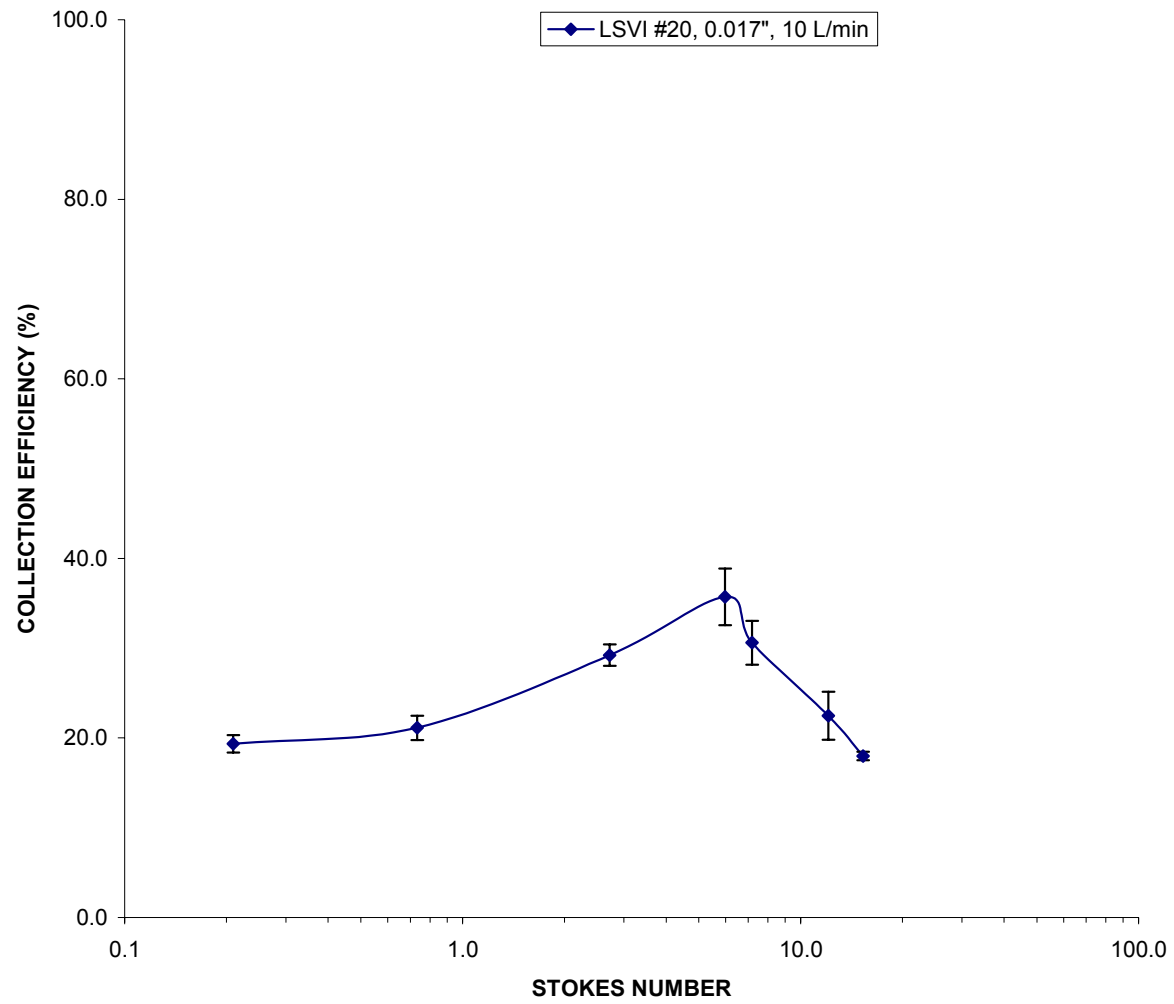


**Figure 34.** Minor flow collection efficiency vs. Stk for LSVI #20 at 10 L/min.



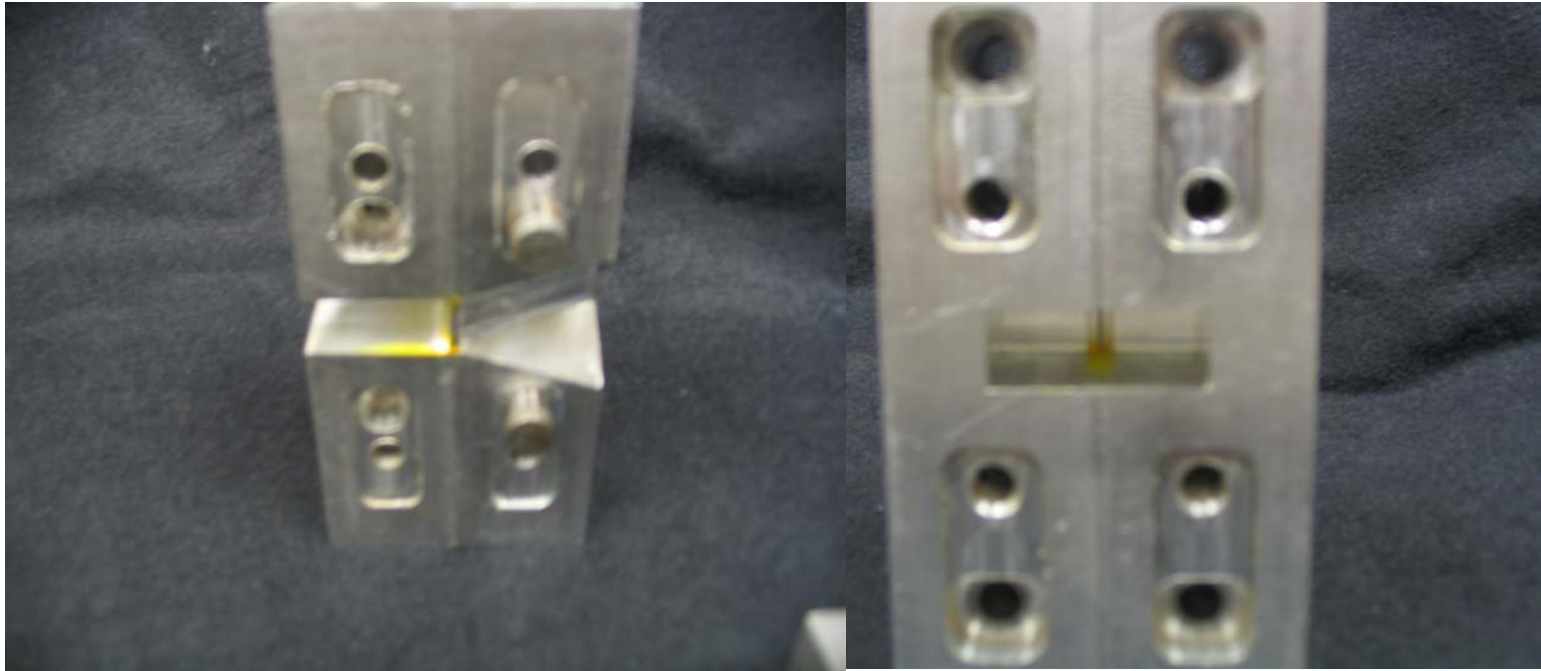


**Figure 35.** Deposition of 3.3  $\mu\text{m}$  particles on the throat ends of LSVI #20.

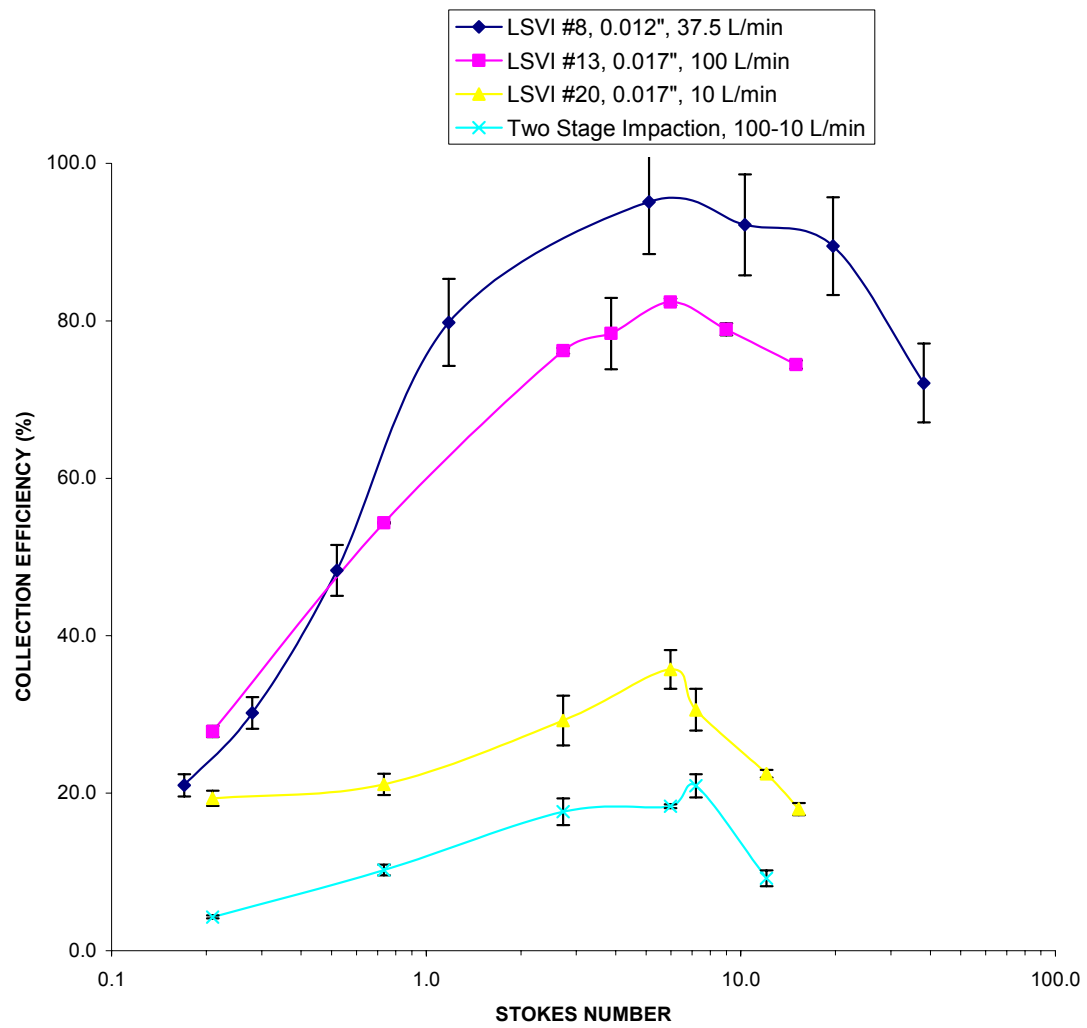


**Figure 36.** Minor flow collection efficiency vs. Stk for second arrangement against previous impactor results.

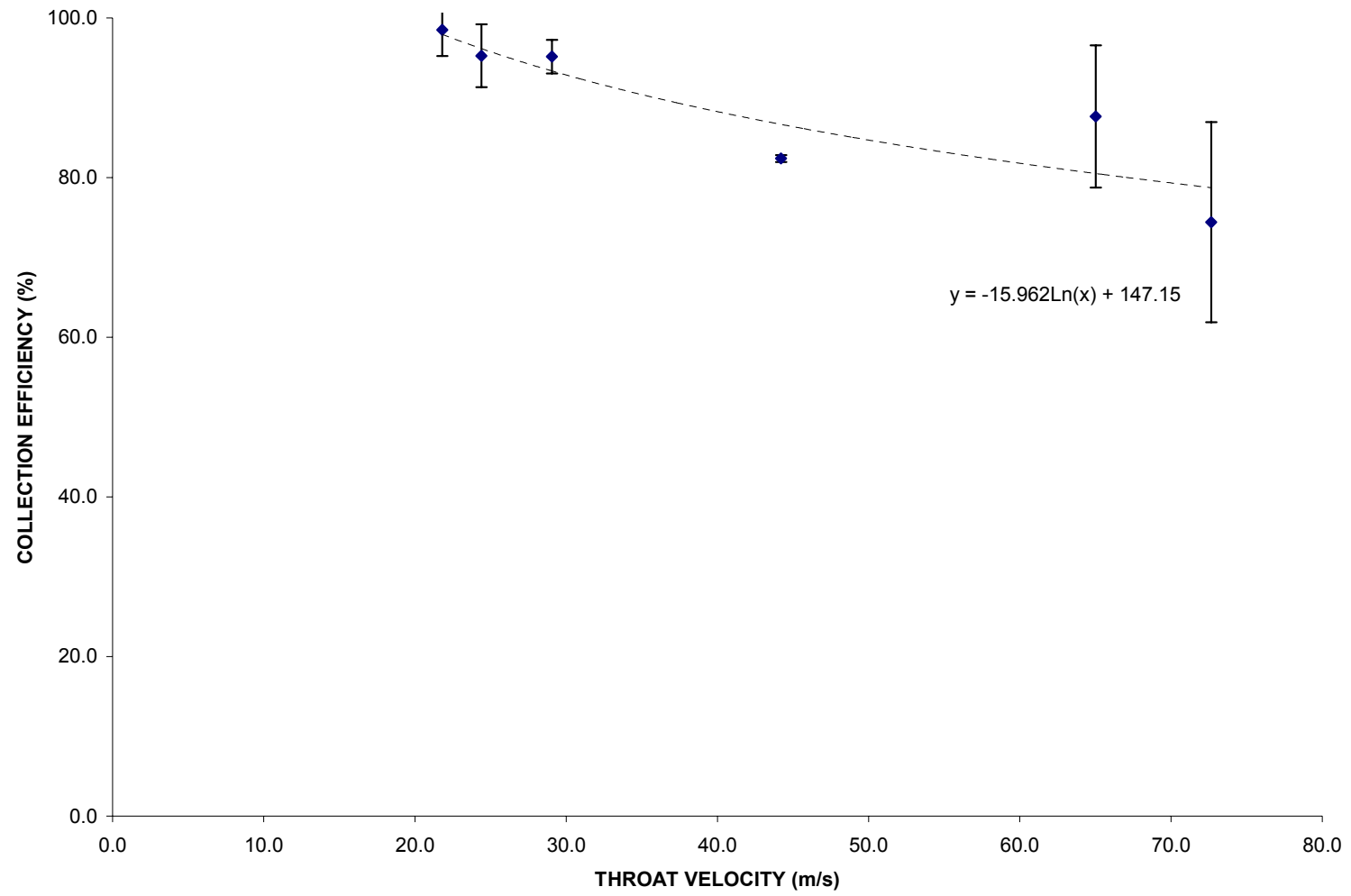


**Figure 37.** Peak minor flow collection efficiency vs. throat velocity for all tested flow rates.

## VITA

Name: Shawn Charles Conerly

Date and Place of Birth: 04/03/1973  
Houston, Texas

Permanent Address: 3510 Shadowvista Ct  
Houston, TX 77082

Education: M.S. Mechanical Engineering (December 2004)  
Texas A&M University  
College Station, TX

B.S. Mechanical Engineering (May 2003)  
The University of Texas at San Antonio  
San Antonio, TX

Work Experience: 9/03-5/05 Graduate Research Assistant  
Aerosol Technology Laboratory  
Mechanical Engineering Department  
Texas A&M University  
College Station, TX 77843

7/99-2/03 Unit Education & Training Manager  
US Air Force  
341 Training Squadron  
Lackland Air Force Base, TX 78236

7/98-7/99 K9 Law Enforcement Patrolman  
US Air Force  
51 Security Forces Squadron  
Osan Air Base, South Korea

12/95-7/98 K9 Law Enforcement Patrolman  
US Air Force  
314 Security Forces Squadron  
Little Rock Air Force Base, AR 72099